

and are ranked according to expression level (high to low). B) HEK-293 cells were treated with TFM-C (50 μ M) for different times and RT-QPCR was performed. Selected genes (*PARK2*, *FBXO4*, *RAB24*, *MAP1LCB3*, *HERP* and *ARMET*) were validated in three independent experiments. The levels of mRNA are shown as 2^{- $\Delta\Delta$ Ct} compared with the level of baseline condition (-) and normalized with the housekeeping gene Glyceraldehyde 3-phosphate dehydrogenase. Asterisks indicate significant differences at **P*<0.05 by Student's test. C) 20 μ g of total protein were loaded for *PARK2*, *FBXO4*, *RAB24*, *MAP1LCB3*, *HERP*, *ARMET* and tubulin Western blot analysis. D) BV2 cells were pre-treated with TFM-C (30 or 50 μ M) for 2h, then stimulated with LPS for different times and 10 μ g of total protein were loaded for Western blot analysis. Results were expressed as arbitrary units compared to the control at same time point. All values represent the averages of three independent experiments. Error bars indicate the standard error. **P*<0.05, ***P*<0.01, ****P*<0.001 by ANOVA test. (TIF)

Figure S3. Quantification of intracellular TNF- α in BV2 cell line. The cells were treated as described in Figure 5 and the fluorescence intensity was analyzed via densitometry using a fluorescence microscope by calculating mean grey value (pixel intensity) normalized by fixed area (ROI=Region Of Interest; Image J Software). For each condition ten cells/field were analyzed for a total of 4 fields and 40 cells. Error bars indicate the standard error. (TIF)

Figure S4. Quantification of TNF- α in plasma membrane of BV2 cell line. BV2 cells were treated with TFM-C (50 μ M) for 2h and stimulated with LPS (1 μ g/ml) for 3, 6 and 24h in presence or absence of TFM-C. The cells were fixed with PFA and stained for TNF- α . A) Fluorescence intensity was analyzed by densitometry calculating mean pixel intensity normalized by

ROI fixed area (Image J Software). For each condition ten cells/field were analyzed for a total of 4 fields and 40 cells. Error bars indicate the standard error. B) Staining for TNF- α in non-permeabilized cells. Scale bar 5 μ m. (TIF)

Figure S5. Normalization of protein expression. BV2 cells were treated with TFM-C (50 μ M) for different times and 10 μ g of total protein were loaded in Stain-free Precast Gels and then transferred to nitrocellulose membrane. A) Total protein was visualized by UV excitation. B) Tubulin protein expression analyzed by Western blot. C) Quantification of HERP band intensity normalized with total protein loaded. D) Quantification of HERP band intensity normalized with Tubulin protein. The values represent the averages of three independent experiments. Significant differences at **P*<0.05 and ***P*<0.01 compared with control (0h) by Student's test. (TIF)

Acknowledgements

Technical and human support provided by SGIker (UPV/EHU, MICINN, GV/EJ, ESF) is gratefully acknowledged for cytometry and confocal microscopy.

Author Contributions

Performed the experiments: AdP AC AW. Analyzed the data: AdP AC IA TY PV SM KV. Contributed reagents/materials/analysis tools: KV PV SM TY. Wrote the manuscript: AdP AC SM KV. Carried out the microscopy, molecular studies, organotypic cultures, EAE model and performed the statistical analysis: AdP AC. Performed astrocytes cultures: AW. Participated in the design and interpretation of the study: AdP AC IA PV SM TY KV. Read and approved the final manuscript: AdP AC IA AW PV SM TY KV.

References

- Shi S, Klotz U (2008) Clinical use and pharmacological properties of selective COX-2 inhibitors. *Eur J Clin Pharmacol* 64: 233-252. doi: 10.1007/s00228-007-0400-7. PubMed: 17999057.
- DeWitt DL (1999) Cox-2-selective inhibitors: the new super aspirins. *Mol Pharmacol* 55: 625-631. PubMed: 10101019.
- Grösch S, Tegeder I, Niederberger E, Bräutigam L, Geisslinger G (2001) COX-2 independent induction of cell cycle arrest and apoptosis in colon cancer cells by the selective COX-2 inhibitor celecoxib. *FASEB J* 15: 2742-2744. PubMed: 11606477.
- Kulp SK, Yang YT, Hung CC, Chen KF, Lai JP et al. (2004) 3-phosphoinositide-dependent protein kinase-1/Akt signaling represents a major cyclooxygenase-2-independent target for celecoxib in prostate cancer cells. *Cancer Res* 64: 1444-1451. doi: 10.1158/0008-5472.CAN-03-2396. PubMed: 14973075.
- Alloza I, Baxter A, Chen Q, Matthiesen R, Vandenbroeck K (2006) Celecoxib inhibits interleukin-12 alpha and beta2 folding and secretion by a novel COX2-independent mechanism involving chaperones of the endoplasmic reticulum. *Mol Pharmacol* 69: 1579-1587. doi:10.1124/mol.105.020669. PubMed: 16467190.
- McLaughlin M, Alloza I, Quoc HP, Scott CJ, Hirabayashi Y et al. (2010) Inhibition of secretion of interleukin (IL)-12/23 family cytokines by 4-trifluoromethyl-celecoxib is coupled to degradation via the endoplasmic reticulum stress protein HERP. *J Biol Chem* 285: 6960-6969. doi: 10.1074/jbc.M109.056614. PubMed: 20054003.
- Vandenbroeck K, Alloza I, Brehmer D, Billiau A, Proost P et al. (2002) The conserved helix C region in the superfamily of interferon-gamma / interleukin-10-related cytokines corresponds to a high-affinity binding site for the HSP70 chaperone DnaK. *J Biol Chem* 277: 25668-25676. doi:10.1074/jbc.M202984200. PubMed: 11970958.
- Vandenbroeck K, Martens E, Alloza I (2006) Multi-chaperone complexes regulate the folding of interferon-gamma in the endoplasmic reticulum. *Cytokine* 33: 264-273. doi:10.1016/j.cyt.2006.02.004. PubMed: 16574426.
- McLaughlin M, Vandenbroeck K (2011) The endoplasmic reticulum protein folding factory and its chaperones: new targets for drug discovery? *Br J Pharmacol* 162: 328-345. doi:10.1111/j.1476-5381.2010.01064.x. PubMed: 20942857.
- Johnson AJ, Hsu AL, Lin HP, Song X, Chen CS (2002) The cyclooxygenase-2 inhibitor celecoxib perturbs intracellular calcium by inhibiting endoplasmic reticulum Ca²⁺-ATPases: a plausible link with its anti-tumour effect and cardiovascular risks. *Biochem J* 366: 831-837. PubMed: 12076251.
- Kardosh A, Golden EB, Pyrko P, Uddin J, Hofman FM et al. (2008) Aggravated endoplasmic reticulum stress as a basis for enhanced glioblastoma cell killing by bortezomib in combination with celecoxib or its non-coxib analogue, 2,5-dimethyl-celecoxib. *Cancer Res* 68: 843-851. doi:10.1158/0008-5472.CAN-07-5555. PubMed: 18245486.
- Okada T, Yoshida H, Akazawa R, Negishi M, Mori K (2002) Distinct roles of activating transcription factor 6 (ATF6) and double-stranded RNA-activated protein kinase-like endoplasmic reticulum kinase (PERK) in transcription during the mammalian unfolded protein

- response. *Biochem J* 366: 585–594. doi:10.1042/BJ20020391. PubMed: 12014989.
13. Oyadomari S, Mori M (2004) Roles of CHOP/GADD153 in endoplasmic reticulum stress. *Cell Death Differ* 11: 381–389. doi:10.1038/sj.cdd.4401373. PubMed: 14685163.
 14. Ni J, Shu YY, Zhu YN, Fu YF, Tang W et al. (2007) COX-2 inhibitors ameliorate experimental autoimmune encephalomyelitis through modulating IFN-gamma and IL-10 production by inhibiting T-bet expression. *J Neuroimmunol* 186: 94–103. doi:10.1016/j.jneuroim.2007.03.012. PubMed: 17442406.
 15. Reder AT, Thapar M, Sapugay AM, Jensen MA (1994) Prostaglandins and inhibitors of arachidonate metabolism suppress experimental allergic encephalomyelitis. *J Neuroimmunol* 54: 117–127. doi:10.1016/0165-5728(94)90238-0. PubMed: 7523442.
 16. Miyamoto K, Miyake S, Mizuno M, Oka N, Kusunoki S et al. (2006) Selective COX-2-inhibitor celecoxib prevents experimental autoimmune encephalomyelitis through COX-2-independent pathway. *Brain* 129: 1984–1992. doi:10.1093/brain/awl170. PubMed: 16835249.
 17. Chiba A, Mizuno M, Tomi C, Tajima R, Alloza I, et al. (2012) A 4-trifluoromethyl analogue of celecoxib inhibits arthritis by suppressing innate immune cell activation. *Arthritis Res Ther* 14: R9.
 18. Trelle S, Reichenbach S, Wandel S, Hildebrand P, Tschannen B et al. (2011) Cardiovascular safety of non-steroidal anti-inflammatory drugs: network meta-analysis. *BMJ* 342: c7086. doi:10.1136/bmj.c7086. PubMed: 21224324.
 19. Ray WA, Varas-Lorenzo C, Chung CP, Castellsague J, Murray KT et al. (2009) Cardiovascular risks of nonsteroidal antiinflammatory drugs in patients after hospitalization for serious coronary heart disease. *Circ Cardiovasc Qual Outcomes* 2: 155–163. doi:10.1161/CIRCOUTCOMES.108.805689. PubMed: 20031832.
 20. Solomon SD, Wittes J, Finn PV, Fowler R, Viner J et al. (2008) Cardiovascular risk of celecoxib in 6 randomized placebo-controlled trials: the cross trial safety analysis. *Circulation* 117: 2104–2113. doi:10.1161/CIRCULATIONAHA.108.764530. PubMed: 18378608.
 21. Feng GS, Ma JL, Wong BC, Zhang L, Liu WD, et al. (2008) Celecoxib-related gastroduodenal ulcer and cardiovascular events in a randomized trial for gastric cancer prevention. *World J Gastroenterol* 14: 4535–4539.
 22. Haag MDM, Bos MJ, Hofman A, Koudstaal PJ, Breteler MMB et al. (2008) Cyclooxygenase selectivity of nonsteroidal anti-inflammatory drugs and risk of stroke. *Arch Intern Med* 168: 1219–1224. doi:10.1001/archinte.168.11.1219. PubMed: 18541831.
 23. Grosser T, Fries S, FitzGerald GA (2006) Biological basis for the cardiovascular consequences of COX-2 inhibition: Therapeutic challenges and opportunities. *J Clin Invest* 116: 4–15. PubMed: 16395396.
 24. Pidgeon GP, Tamosiuniene R, Chen G, Leonard I, Belton O et al. (2004) Intravascular thrombosis after hypoxia-induced pulmonary hypertension: regulation by cyclooxygenase-2. *Circulation* 110: 2701–2707. doi:10.1161/01.CIR.0000145613.01188.0B. PubMed: 15492320.
 25. Buerkle MA, Lehrer S, Sohn H-Y, Conzen P, Pohl U et al. (2004) Selective inhibition of cyclooxygenase-2 enhances platelet adhesion in hamster arterioles in vivo. *Circulation* 110: 2053–2059. doi:10.1161/01.CIR.0000143234.51796.A9. PubMed: 15451781.
 26. Stoppini L, Buchs PA, Muller D (1991) A simple method for organotypic cultures of nervous tissue. *J Neurosci Methods* 37: 173–182. doi:10.1016/0165-0270(91)90128-M. PubMed: 1715499.
 27. Dusart I, Airaksinen MS, Sotelo C (1997) Purkinje cell survival and axonal regeneration are age dependent: an in vitro study. *J Neurosci* 17: 3710–3726. PubMed: 9133392.
 28. Blasi E, Barluzzi R, Bocchini V, Mazzolla R, Bistoni F (1990) Immortalization of murine microglial cells by a v-raf/v-myc carrying retrovirus. *J Neuroimmunol* 27: 229–237. doi:10.1016/0165-5728(90)90073-V. PubMed: 2110186.
 29. McCarthy KD, de Vellis J (1980) Preparation of separate astroglial and oligodendroglial cell cultures from rat cerebral tissue. *J Cell Biol* 85: 890–902. doi:10.1083/jcb.85.3.890. PubMed: 6248568.
 30. Fan LW, Tien LT, Mitchell HJ, Rhodes PG, Cai Z (2008) Alpha-phenyl-n-tert-butyl-nitron ameliorates hippocampal injury and improves learning and memory in juvenile rats following neonatal exposure to lipopolysaccharide. *Eur J Neurosci* 27: 1475–1484.
 31. Kim JY, Shen S, Dietz K, He Y, Howell O et al. (2010) HDAC1 nuclear export induced by pathological conditions is essential for the onset of axonal damage. *Nat Neurosci* 13: 180–189. doi:10.1038/nn.2471. PubMed: 20037577.
 32. Di Penta A, Moreno B, Reix S, Fernandez-Diez B, Villanueva M et al. (2013) Oxidative stress and proinflammatory cytokines contribute to demyelination and axonal damage in a cerebellar culture model of neuroinflammation. *PLOS ONE* 8: e54722. doi:10.1371/journal.pone.0054722.
 33. Sherwin C, Fern R (2005) Acute lipopolysaccharide-mediated injury in neonatal white matter glia: role of TNF-alpha, IL-1beta, and calcium. *J Immunol* 175: 155–161. PubMed: 15972642.
 34. Coleman M (2005) Axon degeneration mechanisms: commonality amid diversity. *Nat Rev Neurosci* 6: 889–898. doi:10.1038/nrn1788. PubMed: 16224497.
 35. Wheeler MC, Rizzi M, Sasik R, Almanza G, Hardiman G, et al. (2008) KDEL-retained antigen in B lymphocytes induces a proinflammatory response: a possible role for endoplasmic reticulum stress in adaptive T cell immunity. *J Immunol* 181: 256–264.
 36. Ron D, Habener JF (1992) CHOP, a novel developmentally regulated nuclear protein that dimerizes with transcription factors C/EBP and LAP and functions as a dominant-negative inhibitor of gene transcription. *Genes Dev* 6: 439–453. doi:10.1101/gad.6.3.439. PubMed: 1547942.
 37. Chung IY, Benveniste EN (1990) Tumor necrosis factor-alpha production by astrocytes. Induction by lipopolysaccharide, IFN-gamma, and IL-1 beta. *J Immunol* 144: 2999–3007.
 38. Johnson AJ, Hsu AL, Lin HP, Song X, Chen CS (2002) The cyclooxygenase-2 inhibitor celecoxib perturbs intracellular calcium by inhibiting endoplasmic reticulum Ca2+-ATPases: a plausible link with its anti-tumour effect and cardiovascular risks. *Biochem J* 366: 831–837. PubMed: 12076251.
 39. Cornell-Bell AH, Finkbeiner SM, Cooper MS, Smith SJ (1990) Glutamate induces calcium waves in cultured astrocytes: long-range glial signaling. *Science* 247: 470–473.
 40. Charles AC, Merrill JE, Dirksen ER, Sanderson MJ (1991) Inter-cellular signaling in glial cells: calcium waves and oscillations in response to mechanical stimulation and glutamate. *Neuron* 6: 983–992. doi:10.1016/0896-6273(91)90238-U. PubMed: 1675864.
 41. Parpura V, Basarsky TA, Liu F, Jeffinija K, Jeffinija S et al. (1994) Glutamate-mediated astrocyte-neuron signalling. *Nature* 369: 744 – 747. doi:10.1038/369744a0. PubMed: 7911978.
 42. Pasti L, Volterra A, Pozzan T, Carmignoto G (1997) Intracellular calcium oscillations in astrocytes: a highly plastic, bidirectional form of communication between neurons and astrocytes in situ. *J Neurosci* 17: 7817–7830. PubMed: 9315902.
 43. Newman EA, Zahs KR (1997) Calcium waves in retinal glial cells. *Science* 275: 844–857. doi:10.1126/science.275.5301.844. PubMed: 9012354.
 44. Bezzi P, Carmignoto G, Pasti L, Vesce S, Rossi D et al. (1998) Prostaglandins stimulate calcium-dependent glutamate release in astrocytes. *Nature* 391: 281–285. doi:10.1038/34651. PubMed: 9440691.
 45. Innocenti B, Parpura V, Haydon PG (2000) Imaging extracellular waves of glutamate during calcium signaling in cultured astrocytes. *J Neurosci* 20: 1800–1808. PubMed: 10684881.
 46. Bezzi P, Domercq M, Brambilla L, Galli R, Schols D et al. (2001) CXCR4-activated astrocyte glutamate release via TNFalpha: amplification by microglia triggers neurotoxicity. *Nat Neurosci* 4: 702–710. doi:10.1038/89490. PubMed: 11426226.
 47. Hoffmann A, Kann O, Ohlemeyer C, Hanisch UK, Kettenmann H (2003) Elevation of basal intracellular calcium as a central element in the activation of brain macrophages (microglia): suppression of receptor-evoked calcium signaling and control of release function. *J Neurosci* 23: 4410–4419.
 48. Meurer R, Van Riper G, Feeney W, Cunningham P, Hora D Jr et al. (1993) Formation of eosinophilic and monocytic intradermal inflammatory sites in the dog by injection of human RANTES but not human monocyte chemoattractant protein 1, human macrophage inflammatory protein 1 alpha, or human interleukin 8. *J Exp Med* 178: 1913–1921. doi:10.1084/jem.178.6.1913. PubMed: 7504053.
 49. Schall TJ, Bacon K, Toy KJ, Goeddel DV (1990) Selective attraction of monocytes and T lymphocytes of the memory phenotype by cytokine RANTES. *Nature* 347: 669–671. doi:10.1038/347669a0. PubMed: 1699135.
 50. Conti P, Reale M, Barbacane RC, Letourneau R, Theoharides TC (1998) Intramuscular injection of hRANTES causes mast cell recruitment and increased transcription of histidine decarboxylase in mice: lack of effects in genetically mast cell-deficient W/WV mice. *FASEB J* 12: 1693–1700. PubMed: 9837859.
 51. Das AM, Ajuebor MN, Flower RJ, Perretti M, McColl SR (1999) Contrasting roles for RANTES and macrophage inflammatory protein-1 alpha (MIP-1 alpha) in a murine model of allergic peritonitis. *Clin Exp Immunol* 117: 223–229. doi:10.1046/j.1365-2249.1999.00978.x. PubMed: 10444251.
 52. Weber C, Weber KS, Klier C, Gu S, Wank R et al. (2001) Specialized roles of the chemokine receptors CCR1 and CCR5 in the recruitment of

- monocytes and T(H)1-like/CD45RO(+) T cells. *Blood* 97: 1144–1146. doi:10.1182/blood.V97.4.1144. PubMed: 11159551.
53. Barnes DA, Huston M, Holmes R, Benveniste EN, Yong VW et al. (1996) Induction of RANTES expression by astrocytes and astrocytoma cell lines. *J Neuroimmunol* 71: 207–214. doi:10.1016/S0165-5728(96)00154-3. PubMed: 8982121.
 54. Selmaj K, Raine CS, Cross AH (1991) Anti-tumor necrosis factor therapy abrogates autoimmune demyelination. *Ann Neurol* 30: 694–700. doi:10.1002/ana.410300510. PubMed: 1722388.
 55. Baker D, Butler D, Scallion BJ, O'Neill JK, Turk JL et al. (1994) Control of established experimental allergic encephalomyelitis by inhibition of tumor necrosis factor (TNF) activity within the central nervous system using monoclonal antibodies and TNF receptor-immunoglobulin fusion proteins. *Eur J Immunol* 24: 2040–2048. doi:10.1002/eji.1830240916. PubMed: 8088324. Available online at: doi:10.1002/eji.1830240916 Available online at: PubMed: 8088324
 56. Hofman FM, Hinton DR, Johnson K, Merrill JE (1989) Tumor necrosis factor identified in multiple sclerosis brain. *J Exp Med*, 170: 607–612. doi:10.1084/jem.170.2.607. PubMed: 2754393.
 57. Sharief MK, Hentges R (1991) Association between tumor necrosis factor-alpha and disease progression in patients with multiple sclerosis. *N Engl J Med* 325: 467–472. doi:10.1056/NEJM199108153250704. PubMed: 1852181.
 58. Probert L, Akassoglou K, Pasparakis M, Kontogeorgos G, Kollias G (1995) Spontaneous inflammatory demyelinating disease in transgenic mice showing central nervous system-specific expression of tumor necrosis factor alpha. *Proc Natl Acad Sci U S A* 92: 11294–11298. doi:10.1073/pnas.92.24.11294. PubMed: 7479982.
 59. Grell M, Wajant H, Zimmermann G, Scheurich P (1998) The type 1 receptor (CD120a) is the high-affinity receptor for soluble tumor necrosis factor. *Proc Natl Acad Sci U S A* 95: 570–575. doi:10.1073/pnas.95.2.570. PubMed: 9435233.
 60. Tracey D, Klareskog L, Sasso EH, Salfeld JG, Tak PP (2008) Tumor necrosis factor antagonist mechanisms of action: a comprehensive review. *Pharmacol Ther* 117: 244–279. doi:10.1016/j.pharmthera.2007.10.001. PubMed: 18155297.
 61. Yang L, Lindholm K, Konishi Y, Li R, Shen Y (2002) Target depletion of distinct tumor necrosis factor receptor subtypes reveals hippocampal neuron death and survival through different signal transduction pathways. *J Neurosci* 22: 3025–3032. PubMed: 11943805.
 62. Suvannavejh GC, Lee HO, Padilla J, Dal Canto MC, Barrett TA et al. (2000) Divergent roles for p55 and p75 tumor necrosis factor receptors in the pathogenesis of MOG (35–55)-induced experimental autoimmune encephalomyelitis. *Cell Immunol* 205: 24–33. doi:10.1006/cimm.2000.1706. PubMed: 11078604.
 63. Kassiotis G, Kollias G (2001) Uncoupling the proinflammatory from the immunosuppressive properties of tumor necrosis factor (TNF) at the p55 TNF receptor level: implications for pathogenesis and therapy of autoimmune demyelination. *J Exp Med* 193: 427–434. doi:10.1084/jem.193.4.427. PubMed: 11181695.
 64. Caminero A, Comabella M, Montalban X (2011) Tumor necrosis factor alpha (TNF- α), anti-TNF- α and demyelination revisited: an ongoing story. *J Neuroimmunol* 234: 1–6. doi:10.1016/j.jneuroim.2011.03.004. PubMed: 21474190.
 65. Bettelli E, Carrier Y, Gao W, Korn T, Strom TB et al. (2006) Reciprocal developmental pathways for the generation of pathogenic effector Th17 and regulatory T cells. *Nature* 441: 235–238. doi:10.1038/nature04753. PubMed: 16648838.
 66. Veldhoen M, Hocking RJ, Atkins CH, Locksley RM, Stockinger B (2006) TGF β in the context of an inflammatory cytokine milieu supports de novo differentiation of mIL-17-producing cells. *Immunity* 24: 179–189. doi:10.1016/j.immuni.2006.01.001. PubMed: 16473830.
 67. de Vries HE, Blom-Roosemalen MC, van Oosten M, de Boer AG, van Berkel TJ et al. (1996) The influence of cytokines on the integrity of the blood-brain barrier in vitro. *J Neuroimmunol* 64: 37–43. doi:10.1016/0165-5728(95)00148-4. PubMed: 8598388.
 68. Cannella B, Raine CS (1995) The adhesion molecule and cytokine profile of multiple sclerosis lesions. *Ann Neurol* 37: 424–435. doi:10.1002/ana.410370404. PubMed: 7536402.
 69. Woodroffe MN, Cuzner ML (1993) Cytokine mRNA expression in inflammatory multiple sclerosis lesions: detection by non-radioactive in situ hybridization. *Cytokine* 5: 583–588. doi:10.1016/S1043-4666(05)80008-0. PubMed: 8186370.
 70. Agnello D, Bigini P, Villa P, Mennini T, Cerami A et al. (2002) Erythropoietin exerts an anti-inflammatory effect on the CNS in a model of experimental autoimmune encephalomyelitis. *Brain Res* 952: 128–134. doi:10.1016/S0006-8993(02)03239-0. PubMed: 12363412.
 71. Eugster HP, Frei K, Kopf M, Lassmann H, Fontana A (1998) IL-6-deficient mice resist myelin oligodendrocyte glycoprotein-induced autoimmune encephalomyelitis. *Eur J Immunol* 28: 2178–2187. doi:10.1002/(SICI)1521-4141(199807)28:07. PubMed: 9692887.
 72. Brett FM, Mizisin AP, Powell HC, Campbell IL (1995) Evolution of neuropathologic abnormalities associated with blood-brain barrier breakdown in transgenic mice expressing interleukin-6 in astrocytes. *J Neuropathol Exp Neurol* 54: 766–775. doi:10.1097/00005072-199511000-00003. PubMed: 7595649.
 73. Castro-Borrero W, Graves D, Frohman TC, Bates Flores A, Hardeman P et al. (2012) Current and emerging therapies in multiple sclerosis: a systematic review. *Ther Adv Neurol Disord* 5: 205–220. doi:10.1177/1756285612450936. PubMed: 22783370.

Nuclear Receptor NR4A2 Orchestrates Th17 Cell-Mediated Autoimmune Inflammation via IL-21 Signalling

Ben J. E. Raveney, Shinji Oki[§], Takashi Yamamura^{*§}

Department of Immunology, National Institute of Neuroscience, National Center of Neurology and Psychiatry, Kodaira, Tokyo, Japan

Abstract

IL-17-producing CD4⁺ T helper 17 (Th17) cells are pathogenic in a range of human autoimmune diseases and corresponding animal models. We now demonstrate that such T cells infiltrating the target organ during the induction of experimental autoimmune encephalomyelitis (EAE) and experimental autoimmune uveoretinitis (EAU) specifically express NR4A2. Further, we reveal a critical involvement of NR4A2 in Th17 cell functions and Th17 cell-driven autoimmune diseases. When NR4A2 expression was blocked with siRNA, full Th17 differentiation was prevented *in vitro*: although cells expressed the master Th17 regulator, ROR γ t, they expressed reduced levels of IL-23R and were unable to produce IL-17 and IL-21. Notably, Th17 differentiation in the absence of NR4A2 was restored by exogenous IL-21, indicating that NR4A2 controls full maturation of Th17 cells via autocrine IL-21 signalling. Preventing NR4A2 expression *in vivo* by systemic treatment with NR4A2-specific siRNA also reduced Th17 effector responses and furthermore protected mice from EAE induction. In addition, the lack of disease was associated with a reduction in autocrine IL-21 production and IL-23R expression. Similar modulation of NR4A2 expression was also effective as an intervention, reversing established autoimmune responses and ameliorating clinical disease symptoms. Thus, NR4A2 appears to control Th17 differentiation and so plays an essential role in the development of Th17-mediated autoimmune disease. As NR4A2 is also upregulated during human autoimmune disease, targeting NR4A2 may provide a new therapeutic approach in treating autoimmune disease.

Citation: Raveney BJE, Oki S, Yamamura T (2013) Nuclear Receptor NR4A2 Orchestrates Th17 Cell-Mediated Autoimmune Inflammation via IL-21 Signalling. PLoS ONE 8(2): e56595. doi:10.1371/journal.pone.0056595

Editor: Martin Stangel, Hannover Medical School, Germany

Received: September 5, 2012; **Accepted:** January 11, 2013; **Published:** February 21, 2013

Copyright: © 2013 Raveney et al. This is an open-access article distributed under the terms of the Creative Commons Attribution License, which permits unrestricted use, distribution, and reproduction in any medium, provided the original author and source are credited.

Funding: This work was supported by the grants from the Ministry of Health, Labour, and Welfare of Japan, the Council for Science and Technology Policy (CSTP) and the Ministry of Education, Science, Culture, Sports, and Technology of Japan. TY is a recipient of a JSPS Grant-in-Aid for Scientific Research (KAKENHI) No. 18109009, SO is a recipient of a JSPS KAKENHI Grant No. 21590087, and BJER was a recipient of a JSPS Postdoctoral Fellowship for Foreign Researchers No. P08517. The funders had no role in study design, data collection and analysis, decision to publish, or preparation of the manuscript.

Competing Interests: The authors have declared that no competing interests exist.

* E-mail: yamamura@ncnp.go.jp

§ These authors contributed equally to this work.

Introduction

T helper (Th) cells responding to self-antigens generate pathogenic inflammatory responses in target organs, leading to local damage and so generate organ-specific autoimmune diseases. It was previously thought that CD4⁺ interferon (IFN)- γ -secreting Th1 cells were critical in inducing autoimmune damage to the central nervous system (CNS) in human multiple sclerosis (MS) and its animal model, experimental autoimmune encephalomyelitis (EAE) [1]. However, the discovery of pathogenic IL-17-secreting Th17 cells as a separate cell lineage opened the door to new research directions towards understanding the development of autoimmune inflammation [2–4]. It is now understood that both Th1 and Th17 cells mediate autoimmune responses in rodents [5–8] as well as in humans [9,10]. Regarding the development of EAE, it has recently been proposed that the major proportion of T cells producing inflammatory cytokines, including IFN- γ , may in fact be T cells that had previously produced IL-17 [11]. Thus, manipulation of Th17 cells might prove effective in controlling complex autoimmune disease processes involving both Th1 and Th17 cells.

Naïve CD4⁺ T cells differentiate into Th1 cells under the influence of IL-12, whereas TGF- β in combination with IL-6 is appreciated as the classical Th17-differentiating cytokine milieu

[12,13]. Recently, however, Th17 differentiation pathways that do not depend on IL-6 or TGF- β have also been described [14–16]. In contrast, *in vivo* studies demonstrate that IL-23 plays a critical role in promoting generation of Th17 cells. Indeed, Th17-mediated autoimmune disease is greatly reduced or prevented in the absence of IL-23 signalling [17,18].

NR4A2, also known as Nurr1, is an orphan nuclear receptor [19–22], and its function in dopaminergic neuron signalling has been widely known. Increasing evidence suggests the role of NR4A2 in inflammatory responses during arthritis and psoriasis [23,24], and NR4A2 may also serve as a regulatory element for reducing immune-mediated tissue damage [25]. We have previously reported that NR4A2 is among the genes expressed by circulating T cells that are highly upregulated in patients with multiple sclerosis (MS) and that NR4A2 is also induced in T cells during rodent EAE [26,27]. We also demonstrated that forced NR4A2 expression enhanced non-specific production of Th1 and Th17 cytokines although further confirmation was needed to confirm the role of NR4A2 in T cell functions.

In this study, we firstly show that NR4A2 is strikingly upregulated by IL-17-secreting Th17 cells infiltrating the target organ of EAE and experimental autoimmune uveoretinitis (EAU), the murine model of posterior uveitis. Using siRNA knockdown techniques, we demonstrate that NR4A2 is dispensable for

induction of the Th17 cell transcription factor ROR γ t in T cells, but is critically required for the *in vitro* generation of fully functional Th17 cells capable of producing IL-17 and IL-21, and expressing the IL-23 receptor (IL-23R). Notably, addition of exogenous IL-21 was able to circumvent the requirement for NR4A2 in Th17 differentiation, and restore the expression of IL-23R and IL-17. Furthermore, NR4A2 knockdown *in vivo* by injection of NR4A2 siRNA either before or after the onset of CNS infiltration ameliorated EAE. Taken together, these data suggest that T cell NR4A2 expression is a hallmark of Th17 cell-mediated pathology and show for the first time that systemic injection of a NR4A2-targeting drug may be a treatment option for Th17-cell mediated diseases.

Materials and Methods

Animals and EAE/EAU Induction

Female C57BL/6J mice (CLEA Laboratory Animal Corp., Tokyo, Japan) aged 8–10 weeks were maintained in specific pathogen-free conditions in accordance with institutional guidelines. This study and all protocols used were approved by the Committee for Small Animal Research and Animal Welfare (National Center of Neurology and Psychiatry). Procedures were carried out under institutional guidelines and all efforts were made to minimize animal suffering. For EAE induction, mice were injected subcutaneously with 100 μ g MOG_{35–55} peptide (synthesized by Toray Research Center, Tokyo, Japan) and 1 mg heat-killed mycobacterium tuberculosis H37RA emulsified in complete Freund's adjuvant (Difco, KS, USA). 200 ng Pertussis toxin (List Biological Laboratories, USA) was injected intraperitoneally (*i.p.*) on days 0 and 2 after immunization. EAE was clinically scored daily (0, no clinical signs; 1, partial tail paralysis; 2, flaccid tail; 3, partial hind limb paralysis; 4, total hind limb paralysis; 5, hind and fore leg paralysis) [28]. EAU was induced as previously described by immunization with 500 μ g human interphotoreceptor binding protein (IRBP)_{1–20} peptide (synthesized by Toray Research Center) in CFA per mouse plus 1 μ g Pertussis toxin [29]. EAU disease severity was monitored by enumeration of the retinal-infiltrating cell number as previously described [30]. Diabetes was induced as previously described [31] by 5 daily *i.p.* doses of 40 mg/kg streptozotocin (STZ; Sigma, Tokyo, Japan) and the urine glucose level was determined daily with Diastix (Bayer, Tokyo, Japan).

siRNA Treatment

NR4A2-specific siRNA (sense – GGACAGCAGUCCUC-CAUUAUUU, anti-sense – UUAUGGAGGACUGCUGUC-CUU) and matching scrambled control sequence siRNA were synthesized by Takara (Shiga, Japan) or Koken (Tokyo, Japan). siRNA was transfected into cells using a mouse CD4 nucleofector kit with an Amaxa electroporator (Lonza, Basel, Switzerland) according to the manufacturer's instructions. For systemic *in vivo* administration, siRNA was stabilized in atelocollagen using an AteloGene kit according to the manufacturer's instructions (Koken) and 10 μ g siRNA per mouse was injected intravenously.

Cell Isolation and Purification

Single cell splenocyte and lymph node cell suspensions were generated by mechanical disruption of tissues. CNS-infiltrating lymphocytes were isolated from spinal cords and brains as previously described [28]. Briefly, tissue was cut into small pieces and digested for 40 minutes at 37°C in RPMI 1640 media (Invitrogen, Tokyo, Japan) supplemented with 1.4 mg/ml Collagenase H and 100 μ g/ml DNase I (Roche, Tokyo, Japan).

Resulting tissue homogenates were forced through a 70 μ m cell strainer and leukocytes were enriched using a discontinuous 37%/70% percoll density gradient centrifugation (GE Healthcare Life Sciences, Tokyo, Japan). Retinal-infiltrating cells and pancreatic-infiltrating cells were isolated by enzymatic digestion as previously described [32,33].

T cells were purified using a CD4 T cell MACS isolation kit with an AutoMACS separator according to the manufacturer's instructions (Miltenyi Biotech, Bergisch Gladbach, Germany). Where required, naive CD4⁺CD44⁻CD25⁻CD62L^{high} T cells or memory CD4⁺CD44⁺CD25⁻CD62L^{low} T cells were further sorted using a FACS ARIA (BD Cytometry Systems, NJ, USA). For sorting of live cytokine-secreting cells, cytokine secretion assay kits (Miltenyi Biotech) were used according to the manufacturer's instructions. Briefly, cells were restimulated with 5 ng/ml PMA +500 ng/ml ionomycin (both Sigma-Aldrich, Tokyo, Japan) and anti-IL-17 and anti-IFN- γ capture antibodies were added for the final 45 minutes of culture. Secondary fluorochrome-conjugated antibodies were added to visualize captured cytokines and cells were sorted using a FACS ARIA flow cytometer.

Cell Culture

Culture media was DMEM supplemented with 10% FCS, 2 mM L-glutamine, 100 U/ml penicillin-streptomycin, and 50 μ M 2-Mercaptoethanol (all Invitrogen). Where indicated, cells were activated with 2 μ g/ml immobilized CD3-specific mAb (2C-11) and 1 μ g/ml CD28-specific mAb (BD Pharmingen, Tokyo, Japan). Polarizing conditions were as follows: Th1, +10 ng/ml IL-12 (PeproTech, London, UK) and 10 μ g/ml IL-4-specific mAb (HB188); Th17, 3 ng/ml TGF- β (R & D Systems, Minneapolis, USA), 20 ng/ml IL-6 (PeproTech), 20 ng/ml IL-23 (R & D Systems), 10 μ g/ml IFN- γ -specific mAb, and 10 μ g/ml IL-4-specific mAb.

Assessment of Cell Function

Cytokine concentrations in supernatants were measured by ELISA as follows: IL-17 using a mouse IL-17 DuoSet (R&D Systems), IL-21 using an IL-21 MaxLegend kit (Biolegend, San Diego, USA), and IFN- γ using a mouse IFN- γ ELISA antibody pair (BD Biosciences). Other cytokines were assessed using a FlowCytomix cytometric bead array (Bender MedSystems, Vienna, Austria) according to the manufacturer's instructions. Proliferation was determined by incubation with [³H]-thymidine (1 μ Ci/well) for the final 12 hours of culture and incorporation of radioactivity was assessed with a β -1205 counter (Pharmacia Biotech, Freiburg, Germany). For intracellular staining, cells were restimulated with 5 ng/ml PMA +500 ng/ml ionomycin (both Sigma-Aldrich) in the presence of Golgi Stop (BD Biosciences) for 5 hours, before surface staining and fixing/intracellular staining using a Foxp3 staining kit (eBioscience, San Diego, CA, USA) according to the manufacturer's instructions. Antibodies were sourced from BioLegend (San Diego, USA), except for anti-cytoplasmic IL-23R (Millipore, Tokyo, Japan).

RNA Extraction and Quantitative RT-PCR

Total RNA was extracted from cell populations using an RNeasy Mini Kit or FastLane kit (Qiagen, Maryland, USA) according to the manufacturer's instructions. cDNA was prepared using a first-strand cDNA Kit (Takara). Quantitative real time PCR was performed with a Light Cycler-FastStart DNA Master SYBR Green I kit using a LightCycler instrument (Roche Diagnostics, Tokyo, Japan) or with a Power SYBR green master

mix using an ABI 7300 real time PCR instrument (Applied Biosystems, Warrington, UK). Primers used were as follows: GAPDH, forward AACGACCCCTTCATTGAC, reverse TCCACATACTCAGCAC; ROR γ t, forward TGTCTGGGCTACCCTACTG, reverse GTGCAGGAGTAGGCCACATT; t-bet, forward GCCAGGGAACCGCTTATATG, reverse GACGATCATCTGGGTCACATTGT; IL-21, forward TCATCATTGACCTCGTGGCCC, reverse ATCGTACTTCCACTTGCAATCCC; IL-23R, forward TCAGTGTACAATCTTCAGAGGACAT, reverse GATGGCCAAGAA-GACCATTCC; IL-17A, forward ATCCCTCAAAGCTCAGCGTGTC, reverse GGGTCTTCATTGCGGTGGAGAG; and Foxp3, forward TTCTCACAACAAGCCACTTG, reverse CCCAGGAAAGCAGCAACCCT. Gene expression values were normalized to the expression of the GAPDH housekeeping gene.

Statistical Analyses

Statistical significance of differences was tested using a Mann Whitney U test unless otherwise stated. $p < 0.05$ was considered significant.

Results

Organ-specific Autoimmune Diseases EAE and EAU Accompany NR4A2 Regulation in T cells

We previously reported T cell expression of NR4A2 during EAE [27]. Here we tested whether or not NR4A2 overexpression is common to T cells involved in autoimmune diseases. We detected NR4A2 upregulation amongst T cells during the development of EAE and EAU, a Th1/Th17-mediated autoimmune disease of the retina: T cell expression of NR4A2 was observed from the earliest stages of both EAE and EAU in CD4⁺ T cell infiltrates in the target organ and, as well as a later NR4A2 upregulation amongst circulating blood CD4⁺ T cells (Fig. 1A&B) after the peak of clinical disease (Fig. S1A&B). Although T cells from secondary lymphoid tissue have the potential to induce EAE or EAU when they are adoptively transferred after being stimulated *in vitro* [34], no significant NR4A2 expression was detected amongst lymph node or splenic T cells at any time examined.

NR4A2 Expression is Associated with IL-17 Producing T cells in EAE

We previously observed that forced expression of NR4A2 in T cells could enhance production of both IL-17 and IFN- γ [27]. However, since this observation was made under non-physiological conditions, we attempted to verify if this finding had physiological meaning *in vivo*. Using a cytokine secretion assay, we separated populations of live CD4⁺ T cells from the blood and CNS of EAE mice based on their production of IFN- γ and IL-17 and measured the expression levels of NR4A2 in each population. Strikingly, in the early phase of EAE, NR4A2 transcripts were detected in those T cells that produced IL-17, either alone or in combination with IFN- γ (Fig. 1C), but not in those that produced IFN- γ alone or neither IFN- γ nor IL-17. Similar findings were observed in T cells isolated from the retina during the early stages of EAU. NR4A2 expression by IL-17-secreting T cells in EAE was detected first in the target organ then later in the blood (Fig. 1D&E), which was concordant with the kinetics of NR4A2 expression in total lymphocytes (Fig. 1A).

NR4A2 Expression is not Detected in STZ-induced Diabetes or following OVA Immunization

We next measured NR4A2 expression in T cells from streptozotocin (STZ)-induced autoimmune diabetes [35], in which autoimmune Th1 cells but not Th17 cells are thought to play a pathogenic role [31]. Repeated administration of low-dose streptozotocin (STZ) induced anti-pancreatic autoimmunity accompanied with clinical diabetes by day 10 (Fig. S1C). Consistent with a previous report [35], splenocytes as well as pancreata-infiltrating T cells produced raised levels of IFN- γ , but not IL-17, after *in vitro* stimulation (Fig. S1D). Unlike CNS-infiltrating T cells in EAE, NR4A2 upregulation was not detected amongst pancreata-infiltrating T cells (Fig. 1F). We also examined blood T cells from these mice and detected no NR4A2 upregulation at any time (Fig. S1E). Furthermore, we examined if NR4A2 upregulation might be induced by active immunization with any antigen in CFA. However, immunization with OVA in CFA, using the same protocol for inducing EAE with MOG peptide, did not lead to NR4A2 upregulation.

NR4A2 Expression is Required for IL-17 Production by ROR γ t⁺ T cells

As NR4A2 expression appeared to be associated with IL-17-secreting pathogenic T cells, we speculated that NR4A2 might function in the process of Th17 cell differentiation. Using NR4A2-specific siRNA, we investigated *in vitro* if CD4⁺ T cells differentiate normally into Th1 or Th17 cells in the absence of NR4A2 regulation. Activation of T cells leads to a rapid and transient upregulation of NR4A2 that could be prevented by transfection with NR4A2 siRNA (Fig. S2A). When NR4A2 expression was silenced in this manner, naive CD4⁺ T cells were able to differentiate into IFN- γ -producing cells (Fig. 2A&C), excluding a requirement for NR4A2 in Th1 cell development. However, blocking NR4A2 upregulation with siRNA greatly reduced Th17 differentiation driven by any concentrations of TGF- β , as assessed by an increase in IL-17 production (Fig. 2B&C), instead there was an increase in IFN- γ -secreting T cells. We also noted that NR4A2 knockdown did not significantly reduce the proliferation of CD4⁺ T cells under any polarizing conditions tested (Fig. S2B), indicating that NR4A2-specific siRNA is unlikely to prevent IL-17 production by affecting cell survival. Intriguingly, despite the lack of IL-17 production in the absence of NR4A2, T cells did upregulate ROR γ t, the hallmark transcription factor of Th17 cells, to levels comparable to fully functional Th17 cells (Fig. 2D).

Lack of IL-17 in the Absence of NR4A2 does not Result from the Action of Foxp3

A previous study has described a failure of ROR γ t-expressing Th17 cells to secrete IL-17 resulting from a direct inhibitory interaction between ROR γ t and the transcription factor Foxp3 [36]. To examine if a similar mechanism, involving Foxp3, is applicable to interpreting our results, we measured the level of Foxp3 expression during NR4A2 knockdown. NR4A2 siRNA did not enhance but reduced Foxp3 expression in both Th17 (TGF- β +IL-6) and regulatory T cell (TGF- β alone) differentiating conditions (Fig. S3A). This finding is consistent with a recent report on a role of NR4A2 for inducing Foxp3 in regulatory T cells [37]. Furthermore, we tested if NR4A2 ablation by siRNA treatment was still effective in preventing IL-17 production when Foxp3 expression was blocked. To do this, we used Foxp3-specific siRNA to prevent Foxp3 expression in T cells that also received either control or NR4A2-specific siRNA. Foxp3 knockdown did not restore IL-17 production in the absence of NR4A2 (Fig. S3B).

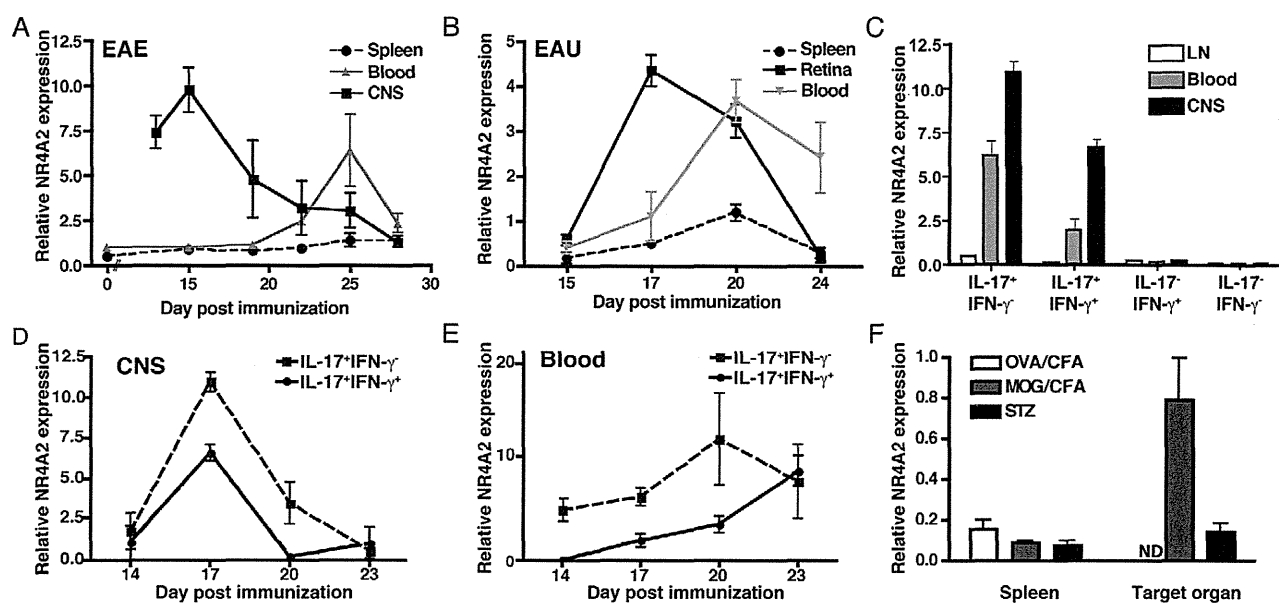


Figure 1. Autoimmune induction of NR4A2 in CD4⁺ T cells is associated with IL-17-secreting T cells. EAE or EAU was induced in C57BL/6 mice by immunization with MOG_{35–55} or IRBP_{1–20} peptide in CFA, respectively. CD4⁺ T cells were purified from spleen, blood, or target organ (CNS or retina) on the indicated days and RNA was isolated. **A** and **B**: NR4A2 expression was quantified by real time PCR relative to GAPDH for T cells from EAE (A) or EAU (B). Timepoints correspond to a minimum of 5 animals and data are representative of 3 independent experiments. CD4⁺ T cells from mice with EAE were restimulated with PMA/ionomycin for 3 hours and 4 populations of cytokine secreting cells (IL-17+IFN- γ ⁻, IL-17+IFN- γ ⁺, IL-17-IFN- γ ⁻, and IL-17-IFN- γ ⁺) were sorted by flow cytometry using IFN- γ and IL-17 cytokine secretion assay kits. **C**: NR4A2 expression by populations of cytokine-secreting CD4⁺ T cells was quantified by real time PCR at day 15 post-EAE induction for lymph nodes (LN) and CNS-infiltrating cells (CNS), and day 25 for blood T cells. **D** and **E**: NR4A2 expression by IL-17⁺IFN- γ ⁻ or IL-17⁺IFN- γ ⁺ CNS-infiltrating T cells (**D**) or blood T cells (**E**) was measured by real time PCR at a range of timepoints. Data are representative of 2 independent experiments. **F**: Th1-mediated diabetes was induced in C57BL/6 mice by 5 daily low dose STZ treatments. Other groups of C57BL/6 mice were immunized with peptides in CFA plus PTX either OVA_{323–339} (OVA/CFA) or MOG_{35–55} (MOG/CFA). On day 22, NR4A2 expression was assessed by real time PCR amongst CD4⁺ T cells from spleen and leukocytes isolated from the relevant target organ (ND, OVA/CFA; CNS, EAE; pancreas, STZ). Timepoints correspond to a minimum of 5 animals and data are representative of 2 independent experiments.
doi:10.1371/journal.pone.0056595.g001

Thus, NR4A2 appears to be required for IL-17 production by Th17 cells, and the underlying mechanism is independent of ROR γ t and Foxp3.

NR4A2 Controls the IL-21-initiated Phase of Th17 Differentiation

ROR γ t expression is required for generation of fully functional Th17 cells. However, when upregulation of NR4A2 is prevented, Th17-polarized ROR γ t⁺ T cells do not acquire the ability to produce IL-17 (Fig. 2). A possible scenario is that ROR γ t regulation is an early event in Th17 differentiation [38], whereas later induction of NR4A2 is critical for inducing signals that promote IL-17 production. IL-21-deficient or IL-21R-deficient T cells resemble NR4A2-deficient T cells in that they express ROR γ t but do not produce IL-17 under Th17 polarizing condition [4,39]. Thus, we suspected that NR4A2 expression might control IL-17 production via autocrine IL-21 signalling. IL-21 is produced during early Th17 cell differentiation and then acts in an autocrine manner to induce IL-23R upregulation by Th17 cells [38,40]; the subsequent action of IL-23 produced by myeloid cells then enhances and stabilizes the Th17 cell phenotype via IL-23R. To clarify the kinetics of these key molecules, we evaluated the expression of IL-21, IL-23R, and IL-17 transcripts by ROR γ t⁺ T cells during *in vitro* Th17 cell differentiation. IL-21 begins to be produced before IL-23R is upregulated, which itself precedes IL-17 expression (Fig. 3A). Interestingly, NR4A2 siRNA transfection strongly inhibited the sequential regulation of IL-21, IL-23R, and

IL-17 RNA transcripts (Fig. 3A). We also confirmed the reduction of IL-21 by NR4A2 siRNA treatment at the protein level (Fig. 3B). These data indicate that NR4A2 may be required for IL-21 production and thus in turn control Th17 differentiation. Furthermore, the lack of NR4A2 also blocked c-maf upregulation (Fig. 3C), a transcription factor reported to control IL-21 expression in Th17 development [41]. Finally, Th17 differentiation yields normal IL-22 production in the absence of NR4A2 (Fig. 3D) and the generation of IL-22 has been shown to be related to pathways downstream of ROR γ t, but independent of c-maf, IL-21, and IL-23 signalling [42]. To test the hypothesis that NR4A2 is required for full Th17 differentiation due to its role in the c-maf/IL-21/IL-23R pathway, we reintroduced this pathway by adding exogenous IL-21 to cultures. Critically, the presence of exogenous IL-21 restored IL-17 secretion by T cells stimulated under Th17 polarizing conditions despite the lack of NR4A2 (Fig. 4A). Additionally, NR4A2-knocked down Th17 cells cultured with IL-21 also expressed equivalent levels of IL-23R to the control Th17 cells (Fig. 4B).

NR4A2 Controls the Severity of EAE

Next we tested if NR4A2 also controlled pathogenic Th17 responses in EAE. Administration of NR4A2-specific siRNA on the day of EAE induction was effective at preventing NR4A2 expression by CNS-infiltrating T cells (Fig. S4A). Such systemic blockade of NR4A2 suppressed the onset of clinical EAE (Fig. 5A), accompanied by a reduced ability of CNS-infiltrating CD4⁺ T

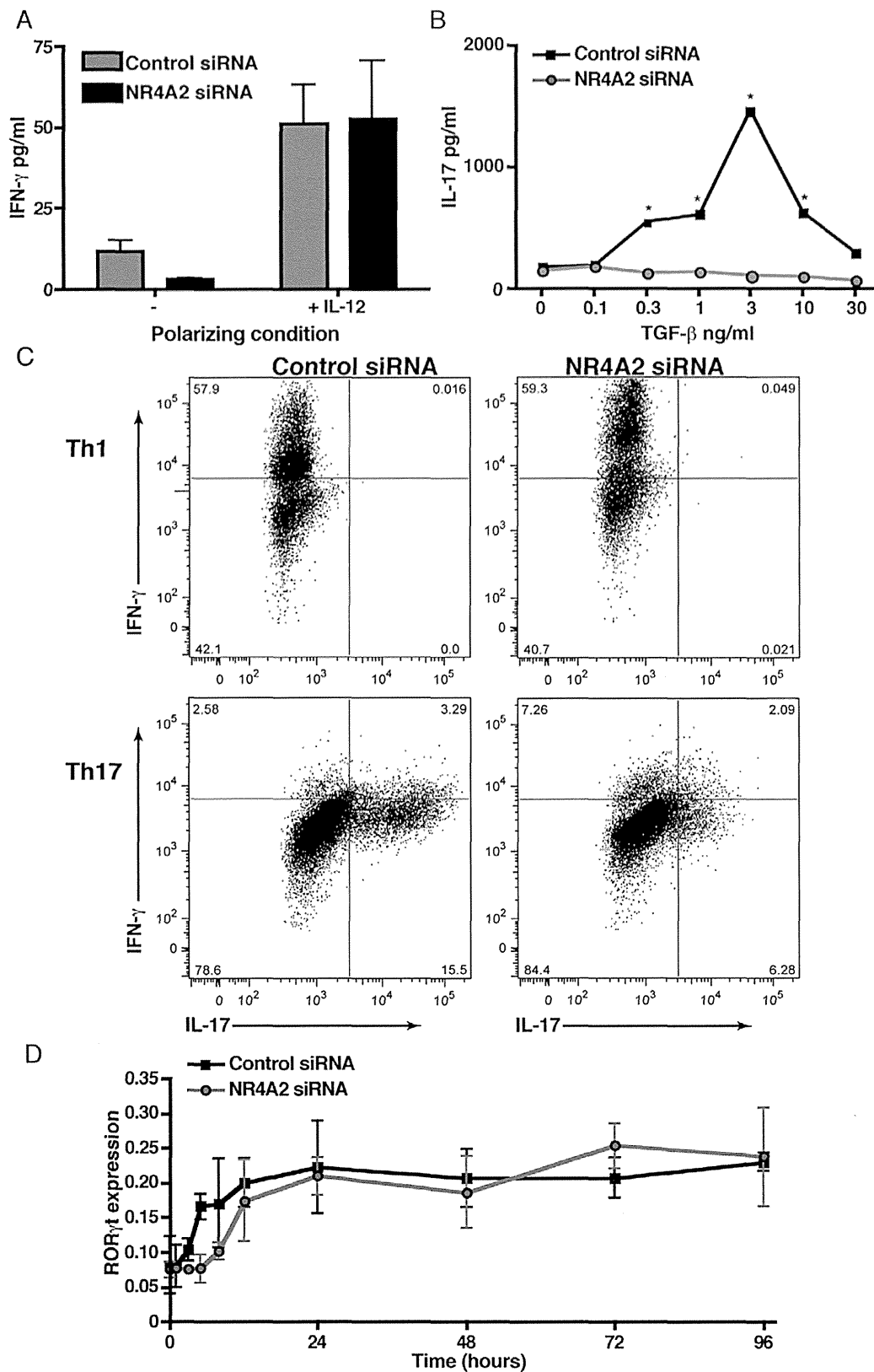


Figure 2. NR4A2 knockdown prevents IL-17 secretion but not ROR γ t upregulation. Naïve CD4⁺ T cells were transfected by electroporation with NR4A2-specific siRNA or scrambled control siRNA. Cells were then activated with 5 μ g/ml plate-bound CD3-specific mAb and 0.5 μ g/ml soluble CD28-specific mAb. **A:** IFN- γ production by cells activated in the presence or absence of 10 ng/ml IL-12 after 96 hours of culture. **B:** IL-17 production

by cells activated in the presence of 20 ng/ml IL-6, 20 ng/ml IL-23, and TGF- β at a range of concentrations after 96 hours of culture. Significant differences between control and NR4A2 siRNA-treatments were tested with a student's t-test, * $p < 0.05$. **C:** IL-17 and IFN- γ intracellular cytokine staining for transfected T cells (control siRNA, left plots; NR4A2 siRNA, right plots) cultured for 96 hours in the presence of 10 ng/ml IL-12 (Th1 conditions, top row plots) or 20 ng/ml IL-6, 20 ng/ml IL-23, and 3 ng/ml TGF- β (Th17 conditions, bottom row plots). **D:** ROR γ t RNA expression as measured by real time PCR by activated T cells cultured under Th17 polarizing conditions at a range of timepoints. Data are representative of 5 independent experiments.

doi:10.1371/journal.pone.0056595.g002

cells to secrete IL-17 but not IFN- γ (Fig. 5B) when restimulated with the immunizing peptide. NR4A2 siRNA treatment also led to a lower proportion of T cells in the target organ that produced IL-17 upon non-specific restimulation during early timepoints (summarized in Fig. 5C; representative data, Fig. S4B). However,

we observed that the effect of NR4A2 siRNA is not persistent, and the mice showed signs of late onset EAE after day 21 (Fig. 5A) accompanied by an increase in the proportion of IL-17 $^+$ T cells in the CNS (Fig. 5C). Since collagen-stabilized siRNA maintains its suppressive activity *in vivo* for approximately three weeks [43], the

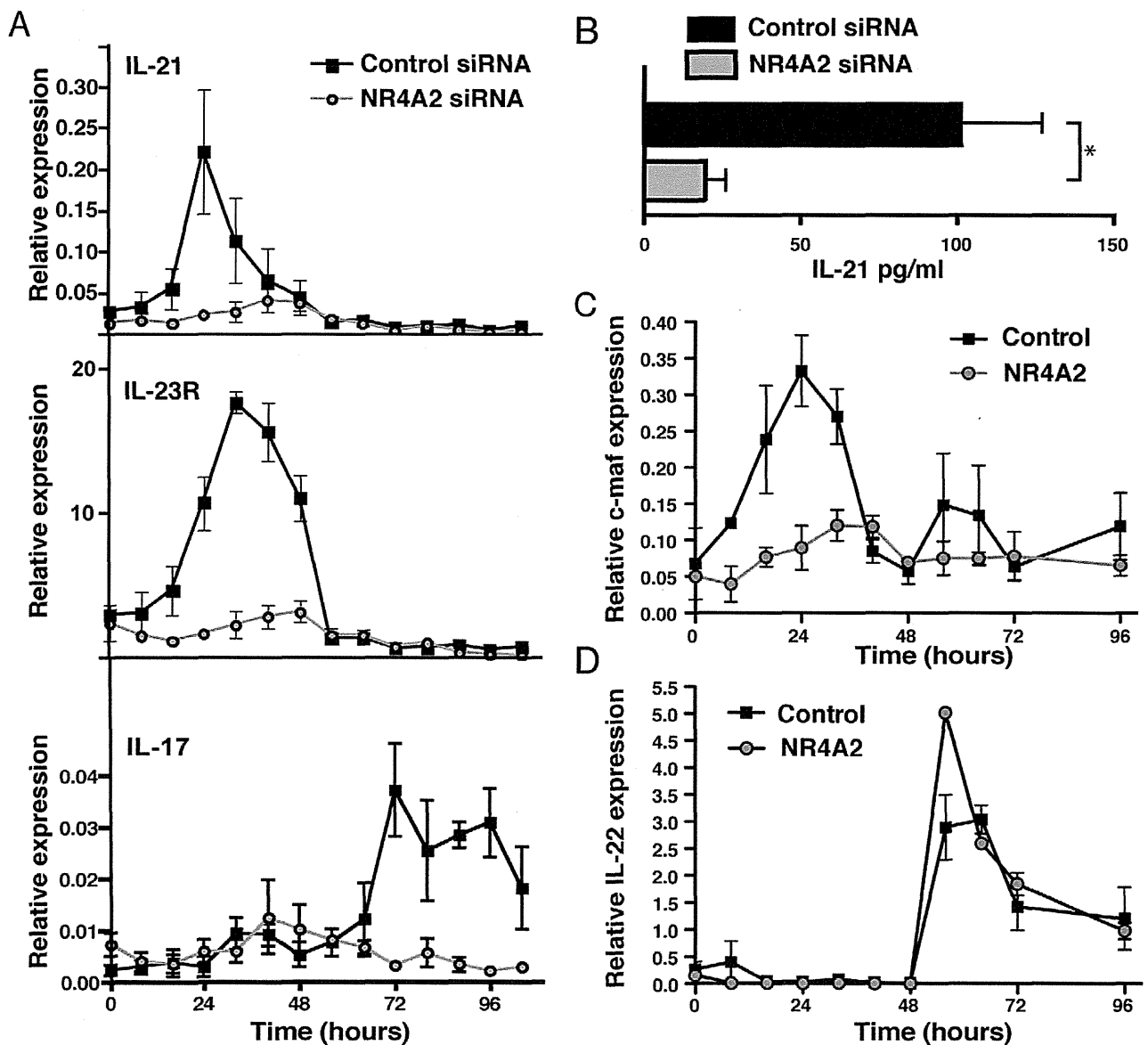


Figure 3. Absence of NR4A2 is associated with a lack of IL-21 production by Th17 cells. Naïve CD4 $^+$ T cells were transfected by electroporation with NR4A2-specific siRNA or scrambled control siRNA and were activated with 5 μ g/ml plate-bound CD3-specific mAb and 0.5 μ g/ml soluble CD28-specific mAb in the presence of 20 ng/ml IL-6, 20 ng/ml IL-23, and 3 ng/ml TGF- β . **A:** RNA levels of IL-21, IL-23R, and IL-17 were quantified by real time PCR at the indicated timepoints following activation. Data are representative of 3 independent experiments. **B:** IL-21 supernatant concentration was measured by ELISA at 96 hours. Data are representative of 3 independent experiments. * $p < 0.05$. **C:** RNA expression of c-maf quantified by real time PCR. **D:** RNA expression of IL-22 quantified by real time PCR. Data are representative of 2 independent experiments. doi:10.1371/journal.pone.0056595.g003

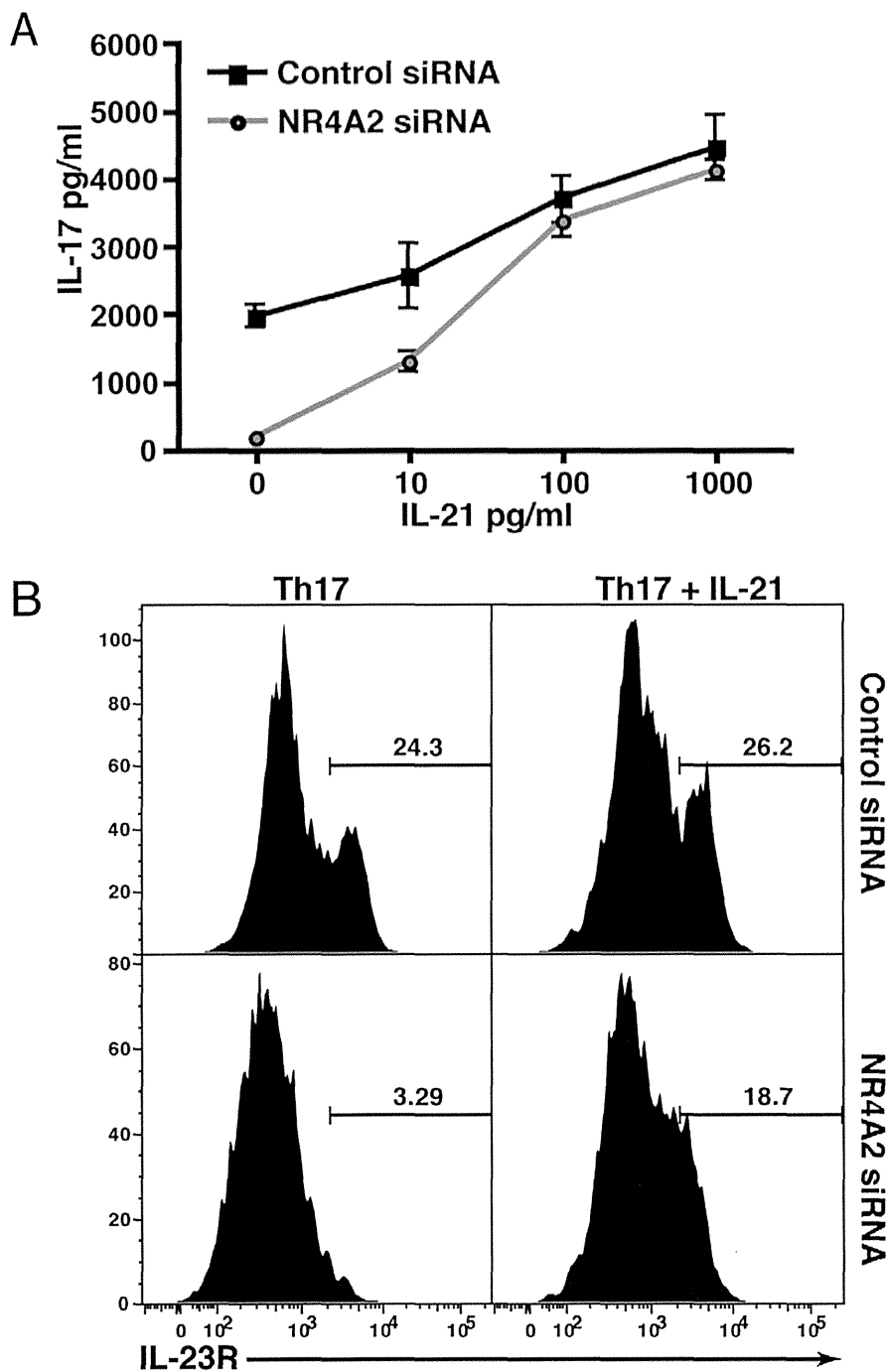


Figure 4. Exogenous IL-21 restores IL-17 production in the absence of NR4A2. Naïve CD4⁺ T cells were transfected by electroporation with NR4A2-specific siRNA or scrambled control siRNA and were activated with 5 µg/ml plate-bound CD3-specific mAb and 0.5 µg/ml soluble CD28-specific mAb in the presence of 20 ng/ml IL-6, 20 ng/ml IL-23, and 3 ng/ml TGF-β. To some wells, recombinant IL-21 was added as indicated. **A:** IL-17 was measured in the supernatants of control or NR4A2 siRNA-treated T cells by ELISA after 96 hours of culture under Th17 polarizing conditions in the presence or absence of IL-21 at the indicated concentrations. **p*<0.05. Data are representative of 3 independent experiments. **B:** IL-23R expression was assessed by intracellular flow cytometric staining after 96 hours of culture under Th17 polarizing conditions in the presence (right plots) or absence (left plots) of 100 pg/ml recombinant IL-21 for control siRNA-treated T cells (top) and NR4A2 siRNA-treated T cells (bottom row). Data are representative of 2 independent experiments. doi:10.1371/journal.pone.0056595.g004

later onset of EAE may reflect the reduced potency of the siRNA. We then tested the effect of injection of NR4A2 siRNA at a later timepoint. Interestingly, when the NR4A2 siRNA was given on

day 10 post-EAE induction, clinical EAE was greatly reduced, and unlike treatment at day 0, no increase in disease was observed after day 20 (Fig. 5D). These results indicate that NR4A2 targeting

siRNA is not only preventative, but also therapeutic against the development of EAE. Furthermore, the CNS-infiltrating T cells also showed reduced expression of IL-21 and IL-23R (Fig. 5E&F), reminiscent of the *in vitro* blocking of NR4A2 during Th17 cell differentiation. Based on these data, we suggest that NR4A2 is a key factor for Th17 differentiation *in vivo* during the initiation of autoimmune responses via its control of IL-21 and IL-23R expression.

Discussion

In this study, we demonstrate that the orphan nuclear receptor NR4A2 is highly expressed by IL-17-secreting T cells infiltrating the target organ of EAE and EAU. When upregulation of NR4A2 was prevented *in vitro*, Th17-polarizing T cells expressing ROR γ t did not further differentiate into mature Th17 cell capable of producing IL-21 and IL-17. This inhibition of Th17 cell differentiation was associated with disruption of autocrine IL-21 signalling. *In vitro* analysis showed that adding exogenous IL-21 restored the ability of the NR4A2 knocked-down Th17 cells to express IL-23R and produce IL-17. Furthermore, *in vivo* injection of NR4A2 siRNA prevented the development of EAE by specifically inhibiting Th17 cell production of IL-17, but not affecting Th1 cells. Based on these findings, we propose that NR4A2 has direct effects on T cell pathogenicity or plays a critical role in continuous new Th17 differentiation and thus it orchestrates effector functions of Th17 cells in mediating autoimmune diseases.

Reagents that dampen the function of Th17 cells are of practical interest in clinical settings. Indeed, an IL-17A-specific antibody was efficacious in clinical trials of human psoriasis, uveitis, and

rheumatoid arthritis [44]. Although the effects of IL-17 blockade on EAE appear to be only modest [45,46], clinical trials are currently in progress to test IL-17A-specific antibody treatment in MS patients. As Th17 cells probably generate a range of proinflammatory cytokines, it is debatable how effective a therapy targeting a single cytokine may prove. NR4A2 appears to control various molecules regulated by IL-21 signalling and therefore a drug targeting NR4A2 may prove more effective than an antibody against a single cytokine.

We previously described that forced expression of NR4A2 in resting T cells led to a modest increase in IFN- γ production following nonspecific stimulation and suggested that NR4A2 might be involved in both Th1 and Th17 cell responses [27]. In contrast, we here reveal that only Th17 cells were found to express NR4A2 in the lesions of EAE, implying that NR4A2 plays a more important role in Th17 cells than in Th1 cells during autoimmune inflammation. However, it is not surprising to see a reduced IFN- γ production in NR4A2 knocked-down T cells *in vitro* (Fig. 2A), since IL-21 has potentials to modulate IFN- γ production under particular conditions [47]. An unexpected report was that the absence of NR4A2 led to increased expression of IFN- γ [37]. The authors argued that the increased production of IFN- γ was due to reduced activity of Foxp3⁺ regulatory T cells that are also dependent on NR4A2 [37]. However, this report does not contradict with our results, because in our *in vitro* experiments, we have explicitly removed regulatory T cells from the starting cell populations.

In agreement with previous studies [17,48], our results showed that autocrine IL-21 production would promote IL-23R expression and subsequent production of IL-17 during Th17 cell

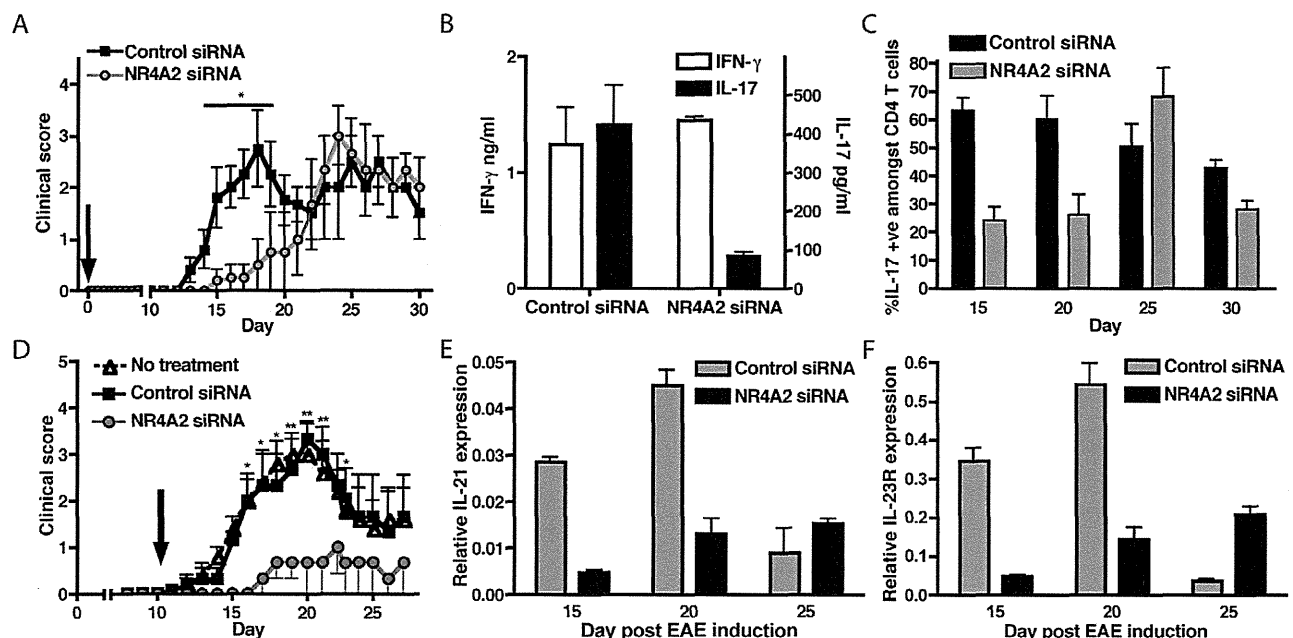


Figure 5. Systemic administration of NR4A2-specific siRNA reduces EAE severity. siRNA, either NR4A2-specific or control, was stabilized in a collagen matrix and administered *i.v.* to groups of C57BL/6 mice at the time of EAE induction. EAE was scored clinically (A) and at day 15 post-EAE induction, production of IL-17 and IFN- γ by CNS-infiltrating leukocytes restimulated with 20 μ g/ml MOG peptide for 96 hours were assessed by ELISA (B). CNS-infiltrating T cells were also assessed for IL-17 production at a range of timepoints by intracellular flow cytometry (C). Data are representative of 3 independent experiments. Control or NR4A2-specific siRNA was applied to MOG-immunized mice at day 10 post-disease induction and disease was scored clinically (D). Timepoints correspond to a minimum of 5 animals and data are representative of 2 independent experiments. IL-21 and IL-23R expressions amongst CNS-infiltrating T cells were measured by real time PCR (E&F). Data are representative of 2 independent experiments. Clinical scores in panels A) and D) were tested with a two-way ANOVA test. * $p < 0.01$, ** $p < 0.001$. doi:10.1371/journal.pone.0056595.g005

differentiation. When NR4A2 upregulation was blocked by siRNA treatment, the production of IL-17 was greatly reduced, although ROR γ t expression was maintained, but exogenously added IL-21 restored IL-17 and IL-23R expression. Furthermore, NR4A2 also appeared to be required for the induction of the transcription factor that controls IL-21 secretion following Th17 differentiation, c-maf [41]. Moreover, lack of NR4A2 had little effect on ROR γ t expression, implying that this transcription factor is not associated with an IL-21-related pathway. It is interesting that IL-22 production is also maintained in the absence of NR4A2, despite the lack of IL-23R, suggesting that this cytokine could be produced via IL-23-independent pathways. TGF- β signals usually inhibit IL-22 production [16], however it is conceivable that these inhibitory signals are ineffective without NR4A2, thus allowing IL-22 secretion in the absence of increased IL-23R expression. Thus, NR4A2 modulation of Th17 cells may be limited to a role in the c-maf/IL-21 pathway, which ultimately controls IL-23R regulation and subsequent signalling. Given the critical role of IL-23 during pathogenic Th17 cell differentiation [16], the ability of NR4A2 siRNA to affect IL-23R expression by inhibiting IL-21 production cannot be ignored. It has been shown that IL-21 can drive Th17 differentiation [49] and thus enhance the initiation phase of EAE [50]. Therefore, the NR4A2-IL-21 pathway is particularly interesting as a therapeutic target. On the other hand, although a report claims that IL-21 is essential for Th17 differentiation [39], other reports showed Th17 differentiation in the absence of IL-21, albeit at a reduced level [14], and IL-17 production and EAE induction were not entirely blocked without IL-21 autocrine signals [51,52]. The discrepancy regarding the role of IL-21 in Th17 cell induction remains to be fully understood and it is possible that absence of IL-21 signalling in gene knockout mice may be compensated by an alternative cytokine signalling pathway. However, our data may be explained by direct effects of NR4A2 on IL-23R upregulation as well as on the c-maf/IL-21 pathway.

In conclusion, our findings highlight the application of siRNA *in vivo* to modulate immunologic pathways that generate pathogenic autoimmune responses. Furthermore, our discovery of the key role of NR4A2 signalling in Th17 differentiation and our identification of the involvement of NR4A2 in generating autoimmune response *in vivo* suggest a new target for intervention in Th17-mediated autoimmune disease. This view is supported by our direct demonstration that manipulation of NR4A2 expression by siRNA treatment in established disease ameliorated clinical symptoms. Thus, future therapies targeting NR4A2 may prove highly effective in treating particular autoimmune diseases.

Supporting Information

Figure S1 EAE or EAU was induced in C57BL/6 mice by immunization with MOG_{35–55} or IRBP_{1–20} peptide in CFA. EAE was scored clinically (A). CD4⁺ T cells were purified from the retina on the indicated days, and EAU disease severity was evaluated by flow cytometric enumeration of ocular infiltrates for EAU (B). Timepoints correspond to a minimum of 5 animals and data are representative of 3 independent experiments. A group of C57BL/6 mice received a low dose of STZ daily for 5 days. Clinical diabetes was tested by measurement of urine glucose level, with diabetes confirmed by consecutive urine glucose result of greater than ≥ 300 mg/dl (C). Plot C shows percentage diabetes. Other groups of C57BL/6 mice were immunized with peptides in CFA plus PTX either OVA_{323–339} (OVA/CFA) or MOG_{35–55} (MOG/CFA). On day 22, splenocytes and leukocytes isolated from the relevant target organ (ND, OVA/CFA; CNS,

EAE; pancreas, STZ) were restimulated with 20 mg/ml of the immunizing peptide, or with soluble anti-CD3 (for STZ); after 96 hours, IL-17 and IFN- γ were measured in supernatants by ELISA (D). NR4A2 expression by blood T cells was also measured at a range of timepoints (E). Timepoints correspond to a minimum of 5 animals and data are representative of 2 independent experiments.

(TIF)

Figure S2 Naïve CD4⁺ T cells were transfected by electroporation with NR4A2-specific siRNA or scrambled control siRNA. Cells were then activated with 5 μ g/ml plate-bound CD3-specific mAb and 0.5 μ g/ml soluble CD28-specific mAb in the presence of 20 ng/ml IL-6, 20 ng/ml IL-23, and 3 ng/ml TGF- β . NR4A2 expression was assessed at a range of timepoints by RT PCR (A). Data are representative of 5 independent experiments. Cell proliferation of transfected cells following anti-CD3/anti-CD28 stimulation in the presence of Th1 (+10 ng/ml IL-12), Th17 (+20 ng/ml IL-6, 20 ng/ml IL-23, and 3 ng/ml TGF- β), or in the absence of polarizing cytokines was measured at 96 hours by the incorporation of ³H-thymidine. Data are representative of 2 independent experiments.

(TIF)

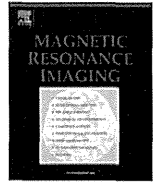
Figure S3 Naïve CD4⁺ T cells transfected by electroporation with NR4A2-specific siRNA or scrambled control siRNA were activated with plate-bound CD3-specific mAb and soluble CD28-specific mAb in the presence of 10 μ g/ml IFN- γ -specific and IL-4-specific mAb, with either 20 ng/ml IL-6, 2 ng/ml TGF- β (IL-6+ TGF- β) or with 10 ng/ml TGF- β (TGF- β). Foxp3 expression at 96 hours as measured by real time PCR is shown in plot A. Data shown represent averages of 4 independent experiments. Naïve CD4⁺ T cells were transfected by electroporation with 2 siRNAs: either Foxp3-specific siRNA or relevant scrambled control siRNA and with either NR4A2-specific siRNA or relevant scrambled control siRNA. This yielded 4 cell types: 1) Foxp3 control/NR4A2 control (C/C); 2) Foxp3 control/NR4A2 siRNA (C/N); 3) Foxp3 siRNA/NR4A2 control (F/C); and 4) Foxp3 siRNA/NR4A2 siRNA (F/N). Cells were then activated with plate-bound CD3-specific mAb and soluble CD28-specific mAb in the presence of 10 μ g/ml IFN- γ -specific and IL-4-specific mAb with either 20 ng/ml IL-6, 2 ng/ml TGF- β (IL-6+ TGF- β) or with 10 ng/ml TGF- β (TGF- β). Plot B shows IL-17 production from each of 4 siRNA-treated cell types at 96 hours as measured by ELISA. Data are representative of 2 independent experiments. siRNA, either NR4A2-specific or control, was stabilized in a collagen matrix and administered *i.v.* to groups of C57BL/6 mice at the time of EAE induction. At the indicated timepoints, CNS-infiltrating T cells were FACS-sorted and NR4A2 expression was assessed by RT PCR (A). CNS-infiltrating leukocytes from day 15 post-EAE induction from control or NR4A2 siRNA-treated mice were restimulated with PMA/ionomycin for 5 hours, and IL-17 and IFN- γ production were visualized by intracellular flow cytometric staining (B). Data are representative of 3 independent experiments (TIF)

Figure S4 siRNA, either NR4A2-specific or control, was stabilized in a collagen matrix and administered *i.v.* to groups of C57BL/6 mice at the time of EAE induction. At the indicated timepoints, CNS-infiltrating T cells were FACS-sorted and NR4A2 expression was assessed by RT PCR (A). CNS-infiltrating leukocytes from day 15 post-EAE induction from control or NR4A2 siRNA-treated mice were restimulated with PMA/ionomycin for 5 hours, and IL-17 and IFN- γ production

were visualized by intracellular flow cytometric staining (B). Data are representative of 3 independent experiments. (TIF)

References

- Sospedra M, Martin R (2005) Immunology of multiple sclerosis. *Annu Rev Immunol* 23: 683–747.
- Bettelli E, Korn T, Kuchroo VK (2007) Th17: the third member of the effector T cell trilogy. *Curr Opin Immunol* 19: 652–657.
- Damsker JM, Hansen AM, Caspi RR (2010) Th1 and Th17 cells: adversaries and collaborators. *Ann N Y Acad Sci* 1183: 211–221.
- Korn T, Oukka M, Kuchroo V, Bettelli E (2007) Th17 cells: effector T cells with inflammatory properties. *Semin Immunol* 19: 362–371.
- Goverman J (2009) Autoimmune T cell responses in the central nervous system. *Nat Rev Immunol* 9: 393–407.
- Jager A, Dardalhon V, Sobel RA, Bettelli E, Kuchroo VK (2009) Th1, Th17, and Th9 effector cells induce experimental autoimmune encephalomyelitis with different pathological phenotypes. *J Immunol* 183: 7169–7177.
- Luger D, Silver PB, Tang J, Cua D, Chen Z, et al. (2008) Either a Th17 or a Th1 effector response can drive autoimmunity: conditions of disease induction affect dominant effector category. *J Exp Med* 205: 799–810.
- Steinman L (2008) A rush to judgment on Th17. *J Exp Med* 205: 1517–1522.
- Man S, Ubogu EE, Ransohoff RM (2007) Inflammatory cell migration into the central nervous system: a few new twists on an old tale. *Brain Pathol* 17: 243–250.
- Matusevicius D, Kivisakk P, He B, Kostulas N, Ozenci V, et al. (1999) Interleukin-17 mRNA expression in blood and CSF mononuclear cells is augmented in multiple sclerosis. *Mult Scler* 5: 101–104.
- Hirota K, Duarte JH, Veldhoen M, Hornsby E, Li Y, et al. (2011) Fate mapping of IL-17-producing T cells in inflammatory responses. *Nat Immunol* 12: 255–263.
- Bettelli E, Carrier Y, Gao W, Korn T, Strom TB, et al. (2006) Reciprocal developmental pathways for the generation of pathogenic effector TH17 and regulatory T cells. *Nature* 441: 235–238.
- Korn T, Bettelli E, Oukka M, Kuchroo VK (2009) IL-17 and Th17 Cells. *Annu Rev Immunol* 27: 485–517.
- Korn T, Bettelli E, Gao W, Awasthi A, Jager A, et al. (2007) IL-21 initiates an alternative pathway to induce proinflammatory T(H)17 cells. *Nature* 448: 484–487.
- Das J, Ren G, Zhang L, Roberts AI, Zhao X, et al. (2009) Transforming growth factor beta is dispensable for the molecular orchestration of Th17 cell differentiation. *J Exp Med* 206: 2407–2416.
- Ghoreschi K, Laurence A, Yang XP, Tato CM, McGeachy MJ, et al. (2011) Generation of pathogenic T(H)17 cells in the absence of TGF-beta signalling. *Nature* 467: 967–971.
- Cua DJ, Sherlock J, Chen Y, Murphy CA, Joyce B, et al. (2003) Interleukin-23 rather than interleukin-12 is the critical cytokine for autoimmune inflammation of the brain. *Nature* 421: 744–748.
- McGeachy MJ, Cua DJ (2007) The link between IL-23 and Th17 cell-mediated immune pathologies. *Semin Immunol* 19: 372–376.
- Law SW, Conneely OM, DeMayo FJ, O'Malley BW (1992) Identification of a new brain-specific transcription factor, NURR1. *Mol Endocrinol* 6: 2129–2135.
- Perlmann T, Wallen-Mackenzie A (2004) Nurr1, an orphan nuclear receptor with essential functions in developing dopamine cells. *Cell Tissue Res* 318: 45–52.
- Le WD, Xu P, Jankovic J, Jiang H, Appel SH, et al. (2003) Mutations in NR4A2 associated with familial Parkinson disease. *Nat Genet* 33: 85–89.
- Pearen MA, Muscat GE (2010) Minireview: Nuclear Hormone Receptor 4A Signaling: Implications for Metabolic Disease. *Mol Endocrinol* 24: 1–13.
- Aherne CM, McMorrow J, Kane D, FitzGerald O, Mix KS, et al. (2009) Identification of NR4A2 as a transcriptional activator of IL-8 expression in human inflammatory arthritis. *Mol Immunol* 46: 3345–3357.
- O'Kane M, Markham T, McEvoy AN, Fearon U, Veale DJ, et al. (2008) Increased expression of the orphan nuclear receptor NURR1 in psoriasis and modulation following TNF-alpha inhibition. *J Invest Dermatol* 128: 300–310.
- Saijo K, Winner B, Carson CT, Collier JG, Boyer L, et al. (2009) A Nurr1/CoREST pathway in microglia and astrocytes protects dopaminergic neurons from inflammation-induced death. *Cell* 137: 47–59.
- Satoh J, Nakanishi M, Koike F, Miyake S, Yamamoto T, et al. (2005) Microarray analysis identifies an aberrant expression of apoptosis and DNA damage-regulatory genes in multiple sclerosis. *Neurobiol Dis* 18: 537–550.
- Doi Y, Oki S, Ozawa T, Hohjoh H, Miyake S, et al. (2008) Orphan nuclear receptor NR4A2 expressed in T cells from multiple sclerosis mediates production of inflammatory cytokines. *Proc Natl Acad Sci U S A* 105: 8381–8386.
- Klemann C, Raveney BJ, Klemann AK, Ozawa T, von Horsten S, et al. (2009) Synthetic retinoid AM80 inhibits Th17 cells and ameliorates experimental autoimmune encephalomyelitis. *Am J Pathol* 174: 2234–2245.
- Raveney BJ, Copland DA, Nicholson LB, Dick AD (2008) Fingolimod (FTY720) as an acute rescue therapy for intraocular inflammatory disease. *Arch Ophthalmol* 126: 1390–1395.
- Copland DA, Wertheim MS, Armitage WJ, Nicholson LB, Raveney BJ, et al. (2008) The clinical time-course of experimental autoimmune uveoretinitis using topical endoscopic fundal imaging with histologic and cellular infiltrate correlation. *Invest Ophthalmol Vis Sci* 49: 5458–5465.
- Mensah-Brown EP, Shahin A, Al-Shamisi M, Wei X, Lukic ML (2006) IL-23 leads to diabetes induction after subdiabetogenic treatment with multiple low doses of streptozotocin. *Eur J Immunol* 36: 216–223.
- Fraser JM, Janicki CN, Raveney BJ, Morgan DJ (2006) Abortive activation precedes functional deletion of CD8+ T cells following encounter with self-antigens expressed by resting B cells in vivo. *Immunology* 119: 126–133.
- Raveney BJ, Copland DA, Dick AD, Nicholson LB (2009) TNFR1-dependent regulation of myeloid cell function in experimental autoimmune uveoretinitis. *J Immunol* 183: 2321–2329.
- Shao H, Liao T, Ke Y, Shi H, Kaplan HJ, et al. (2006) Severe chronic experimental autoimmune uveitis (EAU) of the C57BL/6 mouse induced by adoptive transfer of IRBP1–20-specific T cells. *Exp Eye Res* 82: 323–331.
- Elias D, Prigozin H, Polak N, Rapoport M, Lohse AW, et al. (1994) Autoimmune diabetes induced by the beta-cell toxin STZ. Immunity to the 60-kDa heat shock protein and to insulin. *Diabetes* 43: 992–998.
- Zhou L, Lopes JE, Chong MM, Ivanov II, Min R, et al. (2008) TGF-beta-induced Foxp3 inhibits T(H)17 cell differentiation by antagonizing RORgamma mat function. *Nature* 453: 236–240.
- Sekiya T, Kashiwagi I, Inoue N, Morita R, Hori S, et al. (2011) The nuclear orphan receptor Nr4a2 induces Foxp3 and regulates differentiation of CD4+ T cells. *Nat Commun* 2: 269.
- Zhou L, Ivanov II, Spolski R, Min R, Shenderov K, et al. (2007) IL-6 programs T(H)-17 cell differentiation by promoting sequential engagement of the IL-21 and IL-23 pathways. *Nat Immunol* 8: 967–974.
- Nurieva R, Yang XO, Martinez G, Zhang Y, Panopoulos AD, et al. (2007) Essential autocrine regulation by IL-21 in the generation of inflammatory T cells. *Nature* 448: 480–483.
- Ivanov II, Zhou L, Littman DR (2007) Transcriptional regulation of Th17 cell differentiation. *Semin Immunol* 19: 409–417.
- Bauquet AT, Jin H, Paterson AM, Mitsdoerffer M, Ho IC, et al. (2009) The costimulatory molecule ICOS regulates the expression of c-Maf and IL-21 in the development of follicular T helper cells and TH-17 cells. *Nat Immunol* 10: 167–175.
- Veldhoen M, Hirota K, Westendorp AM, Buer J, Dumoutier L, et al. (2008) The aryl hydrocarbon receptor links TH17-cell-mediated autoimmunity to environmental toxins. *Nature* 453: 106–109.
- Takeshita F, Minakuchi Y, Nagahara S, Honma K, Sasaki H, et al. (2005) Efficient delivery of small interfering RNA to bone-metastatic tumors by using atelocollagen in vivo. *Proc Natl Acad Sci U S A* 102: 12177–12182.
- Hueber W, Patel DD, Dryja T, Wright AM, Koroleva I, et al. (2011) Effects of AIN457, a fully human antibody to interleukin-17A, on psoriasis, rheumatoid arthritis, and uveitis. *Sci Transl Med* 2: 52ra72.
- Hofstetter HH, Ibrahim SM, Koczan D, Kruse N, Weishaupt A, et al. (2005) Therapeutic efficacy of IL-17 neutralization in murine experimental autoimmune encephalomyelitis. *Cell Immunol* 237: 123–130.
- Komiyama Y, Nakae S, Matsuki T, Nambu A, Ishigame H, et al. (2006) IL-17 plays an important role in the development of experimental autoimmune encephalomyelitis. *J Immunol* 177: 566–573.
- Monteleone G, Monteleone I, Fina D, Vavassori P, Del Vecchio Blanco G, et al. (2005) Interleukin-21 enhances T-helper cell type I signaling and interferon-gamma production in Crohn's disease. *Gastroenterology* 128: 687–694.
- Langrish CL, Chen Y, Blumenschein WM, Mattson J, Basham B, et al. (2005) IL-23 drives a pathogenic T cell population that induces autoimmune inflammation. *J Exp Med* 201: 233–240.
- Leonard WJ, Spolski R (2005) Interleukin-21: a modulator of lymphoid proliferation, apoptosis and differentiation. *Nat Rev Immunol* 5: 688–698.
- Vollmer TL, Liu R, Price M, Rhodes S, La Cava A, et al. (2005) Differential effects of IL-21 during initiation and progression of autoimmunity against neuroantigen. *J Immunol* 174: 2696–2701.
- Coquet JM, Chakravarti S, Smyth MJ, Godfrey DI (2008) Cutting edge: IL-21 is not essential for Th17 differentiation or experimental autoimmune encephalomyelitis. *J Immunol* 180: 7097–7101.
- Sonderegger I, Kiselow J, Meier R, King C, Kopf M (2008) IL-21 and IL-21R are not required for development of Th17 cells and autoimmunity in vivo. *Eur J Immunol* 38: 1833–1838.



Abnormalities of cerebral blood flow in multiple sclerosis: A pseudocontinuous arterial spin labeling MRI study[☆]

Miho Ota^{a,*}, Noriko Sato^b, Yasuhiro Nakata^b, Kimiteru Ito^b, Kouhei Kamiya^b, Norihide Maikusa^c, Masafumi Ogawa^d, Tomoko Okamoto^d, Satoko Obu^a, Takamasa Noda^e, Manabu Araki^d, Takashi Yamamura^f, Hiroshi Kunugi^a

^a Department of Mental Disorder Research, National Institute of Neuroscience, National Center of Neurology and Psychiatry, 4-1-1, Ogawa-Higashi, Kodaira, Tokyo 187-8502, Japan

^b Department of Radiology, National Center of Neurology and Psychiatry, 4-1-1, Ogawa-Higashi, Kodaira, Tokyo 187-8551, Japan

^c Department of Imaging Neuroinformatics, Integrative Brain Imaging Center, National Center Hospital of Neurology and Psychiatry, 4-1-1 Ogawa-Higashi, Kodaira, Tokyo 187-8502, Japan

^d Department of Neurology, National Center of Neurology and Psychiatry, 4-1-1, Ogawa-Higashi, Kodaira, Tokyo 187-8551, Japan

^e Department of Psychiatry, National Center of Neurology and Psychiatry, 4-1-1, Ogawa-Higashi, Kodaira, Tokyo 187-8551, Japan

^f Department of Immunology, National Institute of Neuroscience, National Center of Neurology and Psychiatry, 4-1-1, Ogawa-Higashi, Kodaira, Tokyo 187-8502, Japan

ARTICLE INFO

Article history:

Received 20 September 2012

Revised 30 January 2013

Accepted 9 March 2013

Keywords:

Cerebral blood flow
Multiple sclerosis
Pseudocontinuous arterial spin labeling
T2-hyperintense lesion

ABSTRACT

Arterial spin labeling (ASL) is a noninvasive technique that can measure cerebral blood flow (CBF). To our knowledge, there is no study that examined regional CBF of multiple sclerosis (MS) patients by using this technique. The present study assessed the relationship between clinical presentations and functional imaging data in MS using pseudocontinuous arterial spin labeling (pCASL). Twenty-seven patients with MS and 24 healthy volunteers underwent magnetic resonance imaging and pCASL to assess CBF. Differences in CBF between the two groups and the relationships of CBF values with the T2-hyperintense volume were evaluated. Compared to the healthy volunteers, reduced CBF was found in the bilateral thalami and right frontal region of the MS patients. The volume of the T2-hyperintense lesion was negatively correlated with regional CBF in some areas, such as both thalami. Our results suggest that demyelinated lesions in MS mainly have a remote effect on the thalamus and that the measurement of CBF using ASL could be an objective marker for monitoring disease activity in MS.

© 2013 Elsevier Inc. All rights reserved.

1. Introduction

Multiple sclerosis (MS) is a common autoimmune disorder of the central nervous system (CNS) characterized by inflammatory demyelination and secondary axonal degeneration. Although MS has classically been thought of as a typical white matter disorder, the involvement of gray matter regions in the demyelinating process was acknowledged in early pathology studies [1–5], and some hypotheses have been put forward that have explored possible pathogenic processes leading to gray matter damage. These processes could be either primary (arising within gray matter regions) or secondary (pathological changes in gray matter regions that result from continuing damage in the cerebral white matter) and might be intricately connected with each other [6].

Positron emission tomography (PET), single photon emission computed tomography (SPECT) and dynamic susceptibility contrast

(DSC)-enhanced magnetic resonance imaging (MRI) have been used to investigate cerebral metabolic rate, cerebral blood flow (CBF) and cerebral perfusion in MS, respectively. Such imaging techniques have shown significant decreases in areas of white matter, cortical gray matter, subcortical gray matter and normal-appearing white matter [7–16]. However, due to the dissemination of MS lesions in space and time, potential markers for determining their outcomes are poorly understood.

Arterial spin labeling (ASL) MRI is a noninvasive technique that can measure CBF. ASL MRI has two major categories: continuous ASL (CASL) and pulsed ASL (PASL) [17]. The CASL technique uses continuous adiabatic inversion, whereas PASL uses a single inversion pulse. Due to the long steady-state tagging, this technique often has high power disposition and sometimes requires a second radio-frequency (RF) coil for spin labeling [18,19]. Therefore, it has not been widely used compared with PASL, which is simpler in implementation. The recently developed pseudocontinuous ASL (pCASL) MRI is an intermediate technique between CASL and PASL [20–22]. This technique uses a series of discrete RF pulses to mimic the CASL method for spin labeling and brings the potential of combining the

[☆] Conflict of interest: None.

* Corresponding author. Tel.: +81 42 341 2712; fax: +81 42 346 2094.

E-mail address: ota@ncnp.go.jp (M. Ota).

merits of PASL, including less hardware demand and higher tagging efficiency, and CASL, which include a longer tagging bolus and thus a higher signal-to-noise ratio.

ASL measures CBF by taking advantage of arterial water as a freely diffusible tracer, avoiding the need for gadolinium or radioactive ligands; thus, ASL would be a noninvasive and repeatable method of measuring CBF. The ASL technique could be used in place of DSC, PET and SPECT for the examination of neurologic disorders.

We hypothesized that decreased CBF measured by pCASL would, in reflecting neuronal and axonal loss, be associated with the clinical course and disabling forms of MS. In the present study, we assessed the relationship between clinical presentations and functional imaging data in MS using pCASL.

2. Material and methods

2.1. Participant selection

The subjects were 27 patients with MS and 24 healthy controls matched for age, gender and whole brain volume. MS was diagnosed by using previously defined criteria [23]. One female patient out of 27 was the primary progressive MS, and 8 out of 27 (all of them were female, mean age = 47.3 ± 12.9 years) were the secondary progressive MS. No subject had a previous history of any other significant central nervous or systemic autoimmune conditions. The healthy controls were all volunteers without any confirmed neuropsychiatric or major medical illness. All MS subjects underwent a neurological examination to evaluate their Expanded Disability Status Scale (EDSS) scores [24]. The demographic and clinical data of the subjects are shown in Table 1. The study protocol was approved by the Ethics Committee of the National Center of Neurology and Psychiatry, Japan. Informed consent for participation in the study was obtained from all subjects.

2.2. MRI data acquisition and processing

Experiments were performed on a 3-T MR system (Philips Medical Systems, Best, the Netherlands). High spatial resolution, 3-dimensional (3D) T1-weighted images were used for morphometric study. 3D T1-weighted images were acquired in the sagittal plane [repetition time (TR)/echo time (TE), 7.18/3.46; flip angle, 10° ; effective section thickness, 0.6 mm; slab thickness, 180 mm; matrix, 384×384 ; field of view (FOV), 261×261 mm; number of signals acquired, 1], yielding 300 contiguous slices through the brain. In addition to 3D T1-weighted images, we acquired axial T2-weighted turbo spin echo images (TR/TE, 4507/80; slice thickness, 3 mm; intersection gap, 1.5 mm; matrix, 640×640 ; FOV, 230×230 mm; number of signals acquired, 1) and axial fluid-attenuated inversion recovery (FLAIR) images (TR/TE/inversion time, 10,000/120/2650 ms; slice thickness, 3 mm; intersection gap, 1.5 mm; matrix, 512×512 ; FOV, 230×230 mm; number of signals acquired, 1). The imaging parameters for all of the pCASL experiments were identical: single-shot gradient-echo echo planar imaging (EPI) in combination with parallel imaging (SENSE factor 2.0), FOV = 240×240 , ma-

trix = 64×64 , voxel size = 3.75×3.75 mm, 20 slices acquired in ascending order, slice thickness = 7 mm, 1-mm gap between slices, labeling duration = 1650 ms, post spin labeling delay = 1520 ms, TR = 4000 ms, TE = 12 ms, time interval between consecutive slice acquisitions = 32.0 ms, RF duration = 0.5 ms, pause between RF pulses = 0.5 ms, labeling pulse flip angle = 18° , bandwidth = 3.3 kHz/pixel, echo train length = 35. Thirty-two pairs of control/label images were acquired and averaged. The scan duration was 4:24. For measurement of the magnetization of arterial blood and also for segmentation purposes, an EPI M0 image was acquired separately with the same geometry and the same imaging parameters as the pCASL without labeling.

2.3. Postprocessing of the ASL data

Because pCASL and M0 images were acquired separately, both image signal intensities were corrected for data scaling. Corrected data were transferred to a workstation and analyzed using ASLtbx software working on Matlab (Math Works, Natick, MA, USA) [25]. For the CBF calculations, we added the attenuation correction for the transversal relaxation rate of gray matter to the original equation as shown:

$$\begin{aligned} \text{CBF (ml/100 g/min)} &= (6000 * \text{delM} * \text{lamb}) \\ &* \exp(\text{TE} / T_{2,\text{gm}}^* / [2 * \text{alp} * T_{1,\text{blood}} * \text{MOWM} \{ \exp(-w / T_{1,\text{blood}}) \\ &- \exp(-(\text{tau} + w) / T_{1,\text{blood}}) \}]), \end{aligned}$$

Where delM is the difference signal between the control and label acquisitions, lamb is the blood/tissue water partition coefficient, $T_{1,\text{blood}}$ is the longitudinal relaxation time of blood, tau is the labeling time, w is the post labeling delay time, TE is the echo time and $T_{2,\text{gm}}^*$ is the transversal relaxation time of gray matter (assumed to be 44.2 ms) [26]. Alp is the labeling efficiency, and MOWM is the average intensity in the control image within the white matter that was derived from the segmented M0 white matter image calculated using Statistical Parametric Mapping 5 software (SPM5; Wellcome Department of Imaging Neuroscience, London, UK) running on Matlab 7.0. The parameters used in this study were alp = 0.85 (assumed) [17], $T_{1,\text{blood}}$ = 1664 ms (assumed) [27], λ = 0.9 g/ml (assumed) [28], tau = 1.65 s (calculated) and w = 1525 (calculated) ms.

The mean CBF image derived using the ASLtbx software contained some spike noise, and thus, a median filter (a nonlinear digital filtering technique) was used in this study. In median filtering, the neighboring pixels are ranked according to the intensity, and the median value becomes the new value for the central pixel. Since the slice gap that we used was somewhat large, simple 2D median filtering was used. Fig. 1 illustrated the image from the ASL sequence in a single subject. To evaluate CBF voxel-basically, mean CBF images were normalized to the standard space. On the occasion of normalization, each individual 3D-T1 image was first coregistered and resliced to its own M0 image. Next, the coregistered 3D-T1 image was normalized to the "avg152T1" image regarded as the anatomically standard image in SPM5, and then the transformation matrix was applied to the FA maps to normalize them to the standard space. The spatially normalized images were resliced with a final voxel size of approximately $4 \times 4 \times 8$ mm³. Each map was then spatially smoothed with a 4-mm full-width at half-maximum Gaussian kernel in order to decrease spatial noise and compensate for the inexactitude of normalization.

2.4. Measure of volume of T2-hyperintense lesion

The T2-weighted data and FLAIR images for each subject were transferred to the workstation. To measure the accurate volume of the T2-hyperintense lesion, individual T2-weighted data and FLAIR

Table 1
Characteristics of the study sample.

	Healthy volunteers	Multiple sclerosis patients
Male/female	7/17	7/20
Age	38.3 ± 13.2	42.7 ± 13.6
Whole brain volume (L)	1.1 ± 0.1	1.1 ± 0.1
Duration of illness		10.6 ± 9.2
EDSS		4.4 ± 2.5
T2-hyperintense lesion volume (cm ³)		3.4 ± 4.0

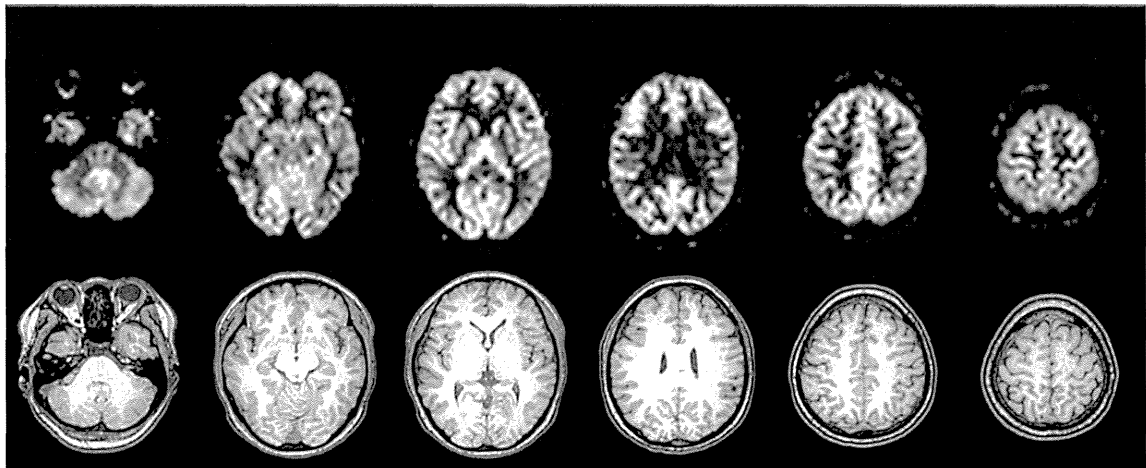


Fig. 1. The upper row showed the typical example of ASL CBF maps acquired in a single healthy volunteer, and lower row showed corresponding slices of T1-weighted image.

data sets were analyzed using QBrain[®]1.1 [22]. The volume quantifications were first performed with manual segmentation and second with the fully automatic segmentation algorithms. Using the software, the T2-hyperintense lesions can be reliably quantified in the milliliter range.

2.5. Measure of whole brain volume

We regarded the gray matter volume plus white matter volume as the whole brain volume. The values of gray and white matter volumes of individual subjects were extracted with the Easy Volume toolbox [29] running on Matlab 7.0. The gray matter and white matter volume images were derived from the segmented 3D-T1 image calculated using SPM5.

2.6. Statistical analysis

We first evaluated the correlations among the EDSS score, age, duration of illness and the ratio of T2-hyperintense lesion volume/

whole brain volume in the MS patients by using Pearson's correlation analysis. Statistical analyses were performed using SPSS Statistics for Windows 17.0 software (SPSS, Tokyo, Japan).

Next, statistical analyses for the CBF were performed using SPM5 software. We evaluated the difference in regional CBF (rCBF) between the MS patients and healthy subjects using age and gender as nuisance variables. Only correlations that met the following criteria were deemed statistically significant: seed levels of $P < .05$ [false discovery rate (FDR) corrected] and a cluster level of $P < .05$ (uncorrected).

Next, correlations between rCBF values and the ratio of T2-hyperintense lesion volume/whole brain volume and between rCBF values and EDSS scores were assessed using age, gender and duration of illness as nuisance variables. Only correlations that met the following criteria were deemed significant: a seed level of $P < .001$ (uncorrected) and a cluster level of $P < .05$ (uncorrected).

Finally, we highlighted the influence of the T2-hyperintense lesion on the CBF. We masked the latter results with the regions for which the results of the former analysis were regarded as significant.

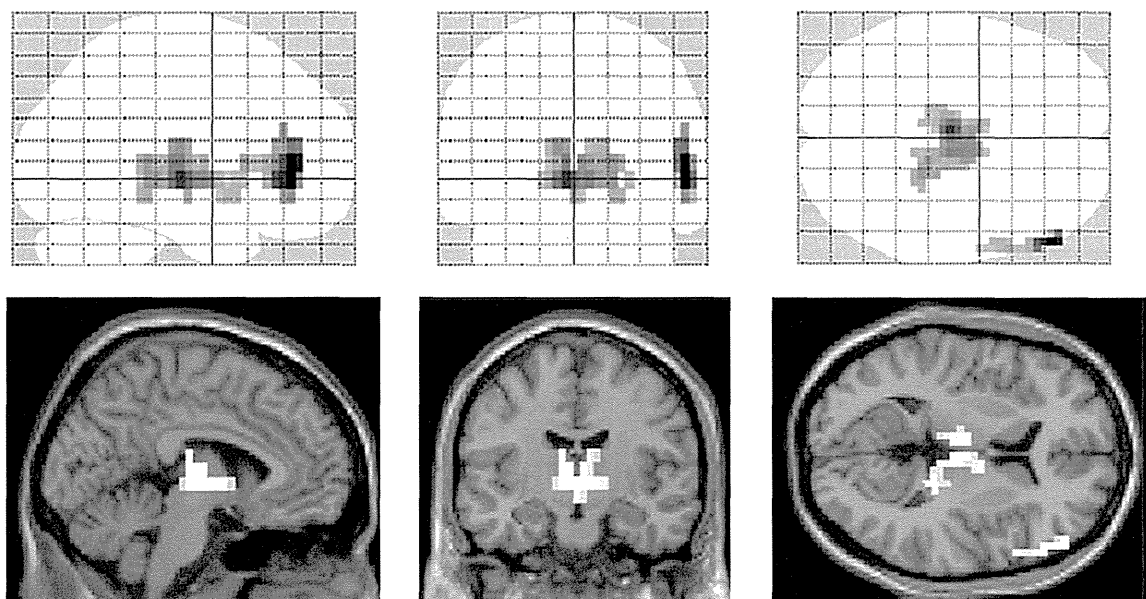


Fig. 2. There were significant reductions of CBF in the right prefrontal cortex and bilateral thalami in the MS patients compared to the healthy controls [$P < .05$ (FDR corrected)].

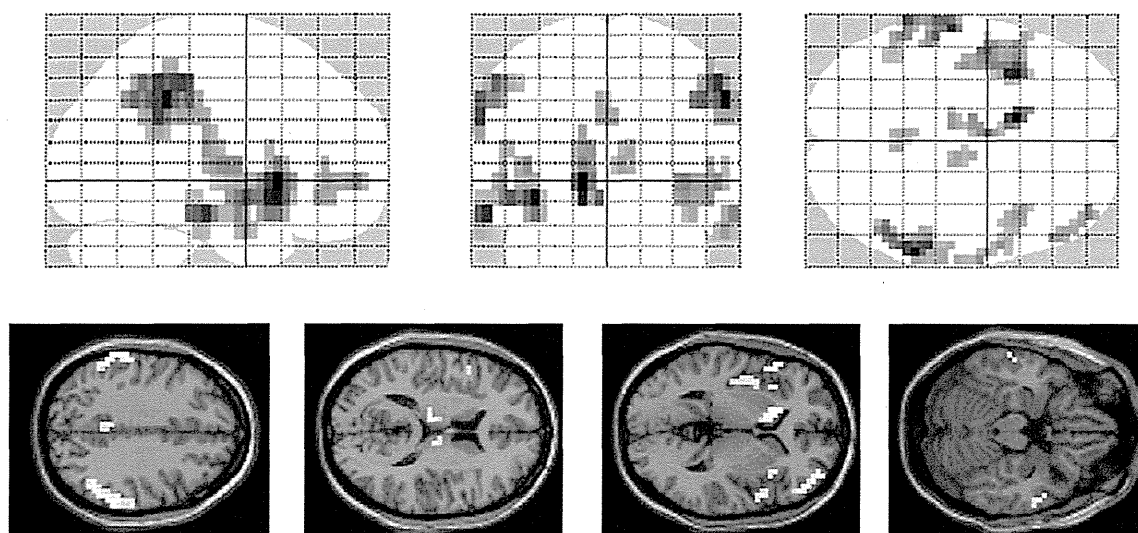


Fig. 3. There were negative correlations between the T2-hyperintense lesion volume/whole brain volume ratio and the regional CBF values in several areas throughout the brain in the MS patients ($P < .001$, uncorrected).

This mask was based on partially the same data of the latter analysis; there existed a multiple testing problem. So, we use the formal thresholding (e.g., FDR) that accounts for this multiplicity [30]. The mask applied the seed levels of $P < .05$ (FDR corrected) as statistically significant.

3. Results

There were no significant correlations between any combinations of two factors of EDSS score, age, duration of illness and the ratio of T2-hyperintense lesion volume/whole brain volume in the MS patients (data not shown). There were significant reductions of CBF in the bilateral thalami and right frontal region of the MS patients compared to the healthy controls (Fig. 2 and Table 2).

There was no increase of CBF in MS patients (data not shown). In the MS patient group, the T2-hyperintense lesion volume/whole brain volume ratio was negatively correlated with rCBF values in the right frontal region, both parietal and temporal regions, both insulae, the left caudate, both thalami and both posterior cinguli (Fig. 3 and Table 3). There were no differences of regional CBF between relapsing–remitting MS patients and secondary progressive MS patients (data not shown).

In contrast, there was no correlation between the EDSS scores and rCBF values (data not shown). There were significant negative correlations between the ratio of the T2-hyperintense lesion volume

to whole brain volume and CBF in both thalami when we masked the second results with the regions in which the results of the first analysis were regarded as significant (Fig. 4).

4. Discussion

To our knowledge, this is the first evaluation of the possible relationships between clinical presentations of MS and CBF using pCASL. By using the pCASL technique, we found significant correlations between the volume of T2-hyperintense lesions and the rCBF values. In particular, CBF in the thalamus was significantly decreased in the patients with MS compared to that of the healthy subjects, and thalamic CBF was correlated with the volume of T2-hyperintense lesion.

There were a few studies of MS using CASL and PASL [14,31]. One study using the CASL showed the reduction of thalamic CBF in MS; however, they did not evaluate the correlation between the volume of T2-hyperintense lesions and the rCBF values [14]. On the other hand, the study using PASL showed not the correlation between them but the correlation between the volume of lesions and mean cortical CBF [31]. These facts may indicate that the CBF study using pCASL calculates the rigorous CBF value. In addition, these studies, including our study, did not show the correlation between the EDSS and rCBF. This may result from the fact that the EDSS mainly focused on the ambulatory ability, not on the higher brain function, so the change of

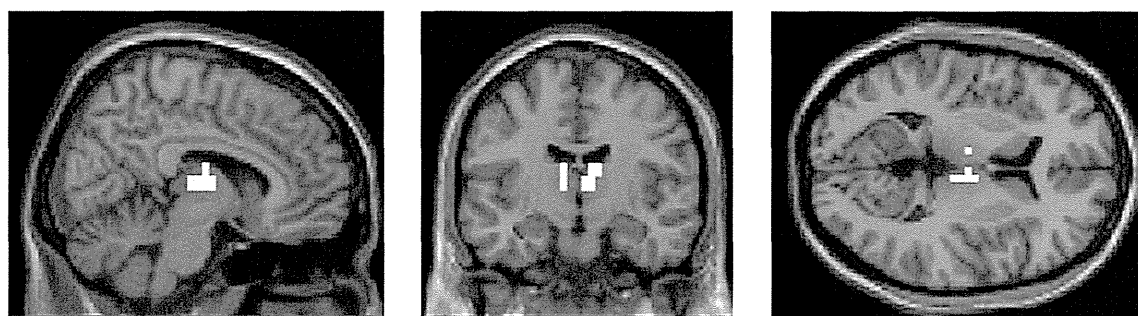


Fig. 4. When the correlation analysis was restricted in both thalami where the CBF reduction was detected in the MS patients, there were significant negative correlations between the T2-hyperintense lesion volume/whole brain volume ratio and the CBF values.

cortical CBF in MS did not reflect the EDSS score. In recent years, the MS Functional Composite (MSFC) was proposed for a new multi-dimensional clinical outcome measure of MS [32]. The MSFC comprises quantitative functional measures of three key clinical dimensions of MS: leg function ambulation, arm/hand function and cognitive function. Further studies with information on MSFC are necessary to address this issue. Additionally, we showed the CBF reduction of the patients with MS in the inferior prefrontal cortex. Previous study showed that MS patients with long duration of disease showed atrophy of the thalami and inferior frontal gyrus [33]. The participants in this study showed relatively long disease duration (Table 1); then the CBF of the patients would show the reduction.

We also found negative correlations between the ratio of the T2-hyperintense lesion volume/whole brain volume and regional CBF in several areas throughout the brain in the MS patients. We focused on volume and not on distribution of the T2-hyperintense lesion in the whole brain, and therefore, the relationship between the volume of lesion and the regional CBF was not examined. However, some previous studies showed reduced metabolism in the prefrontal, parietal and occipital cortex and hippocampus, thalamus, putamen and caudate in MS [7,8,13,14], and those findings are compatible with our results.

Regarding the thalamus, an MRI study of MS patients reported a decrease in thalamic volume and *N*-acetyl aspartate [34]. Those authors also identified the thalamic neuronal loss in MS patients by postmortem examination. Evaluations of the metabolism and perfusion in the brains of patients with MS have also revealed hypometabolism and hypoperfusion in the thalamus [9,12,14]. Furthermore, PET metabolic studies suggest a possible correlation between thalamic hypometabolism and cognitive impairment [7], memory disturbance [13] and the volume of deep white matter lesions [8]. The decreased thalamic CBF observed in our study is consistent with the findings of these previous studies. Another study using diffusion tensor imaging revealed the fine neural networks in the CNS [35]. The thalamus is regarded as the central relay station of the brain, and the reciprocal influence between the thalamus and its associated areas has been well described [36]. The decreased CBF that we observed in the thalamus of the MS patients may be an indication of a disconnection between cortical regions and subcortical relay systems due to the lesion process in MS.

There were some limitations of this study. First, we dealt with the whole brain CBF images, including the gray matter and white matter, voxel-basically. However, we could not detect the white matter CBF change. Previous study showed that the female patients with MS showed the change of white matter compared with men, while gender did not impact gray matter atrophy [33]. Along with the dissemination of MS lesions in space and time, co-gender participants may influence on our results. Further work with single-gender MS patients will be necessary to confirm our results. Second, we did not classify the participants into the three subgroups of MS. The subgroups of MS were defined by the clinical course of illness, and this is not for a cross-sectional study containing the first episode of illness. Not only our study but also two previous cross-sectional studies using ASL also did not show the differences among the

Table 2

Regions that showed significant differences in cerebral blood flow between the patients with multiple sclerosis ($n = 27$) and healthy controls ($n = 24$) using age and gender as nuisance variables.

Cluster size	Z score	x	y	z	Brain region
35	5.17	56	40	8	Right frontal lobe
114	4.61	-4	-16	0	Left thalamus
4	4	8	-16	0	Right thalamus

Table 3

Regions of significant negative correlations between cerebral blood flow and T2-hyperintense lesion volume in MS patients using age, gender and duration of illness as nuisance variables.

Cluster size	Z score	x	y	z	Brain region
16	3.62	40	56	0	Right frontal lobe
35	3.98	-64	-44	32	Left parietal lobe
49	4.33	60	-40	40	Right parietal lobe
11	4.17	-60	-20	-16	Left temporal lobe
9	3.61	64	-4	-16	Right temporal lobe
68	4.29	-36	16	-8	Left insula
24	3.59	56	8	0	Right insula
23	4.59	-12	16	0	Left caudate
11	3.55	-12	-8	8	Left thalamus
9	3.42	8	-16	8	Right thalamus
12	3.37	4	-48	32	Right posterior cingulate
	3.33	-4	-44	40	Left posterior cingulate

subgroups of MS [14,31]. Further longitudinal work would show the difference among the subgroups. A third limitation of the present study is that we did not eliminate the effect of immunomodulating treatment on CBF. Further work with drug-free MS patients will be necessary to confirm our results.

In conclusion, our findings indicate that the noninvasive pCASL is a useful technique which demonstrated that regional CBF values are closely related to the brain lesions in MS. In addition, our results suggest that the demyelinating lesions in MS mainly have a remote effect on the function of the thalamus. Measurement of CBF by pCASL MRI has the potential to be an objective marker for monitoring disease activity in MS (Tables 2 and 3).

Acknowledgments


We are grateful to Ms. Yuriko Suzuki at Philips for helpful discussions. This study was supported by Health and Labour Sciences Research Grants (Comprehensive Research on Disability, Health, and Welfare, #H23-seisin-young scientist 013; #H21-kokoro-002), an Intramural Research Grant for Neurological and Psychiatric Disorders of NCNP and "Understanding of molecular and environmental bases for brain health" carried out under the Strategic Research Program for Brain Sciences of the Ministry of Education, Culture, Sports, Science and Technology of Japan.

References

- [1] Brownell B, Hughes JT. The distribution of plaques in the cerebrum in multiple sclerosis. *J Neurol Neurosurg Psychiatry* 1962;25:315–20.
- [2] Dawson JW. The histology of multiple sclerosis. *Trans R Soc (Edinb)* 1916;50:517–740.
- [3] Dinkler M. Zur Kasuistik der multiplen Herdsklerose des Gehirns und Rückenmarks. *Deuts Zeits f Nervenheilk* 1904;26:233–47.
- [4] Sander M. Hirnrindenbefunde bei multipler Sklerose. *Monatschrift Psychiatrie Neurol* 1898;IV:427–36.
- [5] Schob F. Ein Beitrag zur pathologischen Anatomie der multiplen Sklerose. *Monatschrift Psychiatrie Neurol* 1907;22:62–87.
- [6] Geurts JJ, Barkhof F. Grey matter pathology in multiple sclerosis. *Lancet Neurol* 2008;7:841–51.
- [7] Blinkenberg M, Rune K, Jensen CV, Ravnborg M, Kyllingsbaek S, Holm S, et al. Cortical cerebral metabolism correlates with MRI lesion load and cognitive dysfunction in MS. *Neurology* 2000;54:558–64.
- [8] Derache N, Marié RM, Constans JM, Defer GL. Reduced thalamic and cerebellar rest metabolism in relapsing-remitting multiple sclerosis, a positron emission tomography study: correlations to lesion load. *J Neurol Sci* 2006;245:103–9.
- [9] Inglese M, Park SJ, Johnson G, Babb JS, Miles L, Jaggi H, et al. Deep gray matter perfusion in multiple sclerosis: dynamic susceptibility contrast perfusion magnetic resonance imaging at 3 T. *Arch Neurol* 2007;64:196–202.
- [10] Law M, Saindane AM, Ge Y, Babb JS, Johnson G, Mannon LJ, et al. Microvascular abnormality in relapsing-remitting multiple sclerosis: perfusion MR imaging findings in normal-appearing white matter. *Radiology* 2004;231:645–52.
- [11] Lycke J, Wikkelso C, Bergh AC, Jacobsson L, Andersen O. Regional cerebral blood flow in multiple sclerosis measured by single photon emission tomography with technetium-99 m hexamethylpropyleneamine oxide. *Eur Neurol* 1993;33:163–7.

- [12] Papadakis EZ, Mastorodemos VC, Amanakis EZ, Tsekouras KC, Papadakis AE, Tsavalas ND, et al. White matter and deep gray matter hemodynamic changes in multiple sclerosis patients with clinically isolated syndrome. *Magn Reson Med* 2012;68:1932–42.
- [13] Paulesu E, Perani D, Fazio F, Comi G, Pozzilli C, Martinelli V, et al. Functional basis of memory impairment in multiple sclerosis: a [18 F]FDG PET study. *Neuroimage* 1996;4:87–96.
- [14] Rashid W, Parkes LM, Ingle GT, Chard DT, Toosy AT, Altmann DR, et al. Abnormalities of cerebral perfusion in multiple sclerosis. *J Neurol Neurosurg Psychiatry* 2004;75:1288–93.
- [15] Saindane AM, Law M, Ge Y, Johnson G, Babb JS, Grossman RI. Correlation of diffusion tensor and dynamic perfusion MR imaging metrics in normal-appearing corpus callosum: support for primary hypoperfusion in multiple sclerosis. *AJNR Am J Neuroradiol* 2007;28:767–72.
- [16] Varga AW, Johnson G, Babb JS, Herbert J, Grossman RI, Inglese M. White matter hemodynamic abnormalities precede sub-cortical gray matter changes in multiple sclerosis. *J Neurol Sci* 2009;282:28–33.
- [17] Aslan S, Xu F, Wang PL, Uh J, Yezhuvath US, van Osch M, et al. Estimation of labeling efficiency in pseudocontinuous arterial spin labeling. *Magn Reson Med* 2010;63:765–71.
- [18] Wolff SD, Balaban RS. Magnetization transfer contrast (MTC) and tissue water proton relaxation in vivo. *Magn Reson Med* 1989;10:135–44.
- [19] Detre JA, Alsop DC. Perfusion magnetic resonance imaging with continuous arterial spin labeling: methods and clinical applications in the central nervous system. *Eur J Radiol* 1999;30:115–24.
- [20] Dai W, Garcia D, de Bazelaire C, Alsop DC. Continuous flow-driven inversion for arterial spin labeling using pulsed radio frequency and gradient fields. *Magn Reson Med* 2008;60:1488–97.
- [21] Wong EC. Vessel-encoded arterial spin-labeling using pseudocontinuous tagging. *Magn Reson Med* 2007;58:1086–91.
- [22] Wu WC, Fernandez-Seara M, Detre JA, Wehrli FW, Wang J. A theoretical and experimental investigation of the tagging efficiency of pseudocontinuous arterial spin labeling. *Magn Reson Med* 2007;58:1020–7.
- [23] Polman CH, Reingold SC, Banwell B, Clanet M, Cohen JA, Filippi M, et al. Diagnostic criteria for multiple sclerosis: 2010 revisions to the McDonald criteria. *Ann Neurol* 2011;69:292–302.
- [24] Kurtzke JF. Rating neurologic impairment in multiple sclerosis: an expanded disability status scale (EDSS). *Neurology* 1983;33:1444–52.
- [25] Wang Z, Aguirre GK, Rao H, Wang J, Fernández-Seara MA, Childress AR, et al. Empirical optimization of ASL data analysis using an ASL data processing toolbox: ASLtbx. *Magn Reson Imaging* 2008;26:261–9.
- [26] Cavuşoğlu M, Pfeuffer J, Uğurbil K, Uludağ K. Comparison of pulsed arterial spin labeling encoding schemes and absolute perfusion quantification. *Magn Reson Imaging* 2009;27:1039–45.
- [27] Lu H, Clingman C, Golay X, van Zijl PC. Determining the longitudinal relaxation time (T₁) of blood at 3.0 tesla. *Magn Reson Med* 2004;52:679–82.
- [28] Wang J, Zhang Y, Wolf RL, Roc AC, Alsop DC, Detre JA. Amplitude-modulated continuous arterial spin-labeling 3.0-T perfusion MR imaging with a single coil: feasibility study. *Radiology* 2005;235:218–28.
- [29] Pernet C, Andersson J, Paulesu E, Demonet JF. When all hypotheses are right: a multifocal account of dyslexia. *Hum Brain Mapp* 2009;30:2278–92.
- [30] Carter CS, Heckers S, Nichols T, Pine DS, Strother S. Optimizing the design and analysis of clinical functional magnetic resonance imaging research studies. *Biol Psychiatry* 2008;64:842–9.
- [31] Amann M, Achtnichts L, Hirsch JG, Naegelin Y, Gregori J, Weier K, et al. 3D GRASE arterial spin labelling reveals an inverse correlation of cortical perfusion with the white matter lesion volume in MS. *Mult Scler* 2012;18:1570–6.
- [32] Fischer JS, Rudick RA, Cutter GR, Reingold SC. The Multiple Sclerosis Functional Composite Measure (MSFC): an integrated approach to MS clinical outcome assessment. National MS Society Clinical Outcomes Assessment Task Force. *Mult Scler* 1999;5:244–50.
- [33] Riccitelli G, Rocca MA, Pagani E, Martinelli V, Radaelli M, Falini A, et al. Mapping regional grey and white matter atrophy in relapsing-remitting multiple sclerosis. *Mult Scler* 2012;18:1027–37.
- [34] Cifelli A, Arridge M, Jezzard P, Esiri MM, Palace J, Matthews PM. Thalamic neurodegeneration in multiple sclerosis. *Ann Neurol* 2002;52:650–3.
- [35] Behrens TE, Johansen-Berg H, Woolrich MW, Smith SM, Wheeler-Kingshott CA, Boulby PA, et al. Noninvasive mapping of connections between human thalamus and cortex using diffusion imaging. *Nat Neurosci* 2003;6:750–7.
- [36] Buffon F, Molko N, Hervé D, Porcher R, Denghien I, Pappata S, et al. Longitudinal diffusion changes in cerebral hemispheres after MCA infarcts. *J Cereb Blood Flow Metab* 2005;25:641–50.

Molecular network of chromatin immunoprecipitation followed by deep sequencing-based vitamin D receptor target genes

Multiple Sclerosis Journal
0(0) 1–11
© The Author(s) 2013
Reprints and permissions:
sagepub.co.uk/journalsPermissions.nav
DOI: 10.1177/1352458512471873
msj.sagepub.com


Jun-ichi Satoh and Hiroko Tabunoki

Abstract

Background: Vitamin D is a liposoluble vitamin essential for calcium metabolism. The ligand-bound vitamin D receptor (VDR), heterodimerized with retinoid X receptor, interacts with vitamin D response elements (VDREs) to regulate gene expression. Vitamin D deficiency due to insufficient sunlight exposure confers an increased risk for multiple sclerosis (MS).

Objective: To study a protective role of vitamin D in multiple sclerosis (MS), it is important to characterize the global molecular network of VDR target genes (VDRTGs) in immune cells.

Methods: We identified genome-wide VDRTGs collectively from two distinct chromatin immunoprecipitation followed by deep sequencing (ChIP-Seq) datasets of VDR-binding sites derived from calcitriol-treated human cells of B cell and monocyte origins. We mapped short reads of next generation sequencing (NGS) data on hg19 with Bowtie, detected the peaks with Model-based Analysis of ChIP-Seq (MACS), and identified genomic locations by GenomeJack, a novel genome viewer for NGS platforms.

Results: We found 2997 stringent peaks distributed on protein-coding genes, chiefly located in the promoter and the intron on VDRE DR3 sequences. However, the corresponding transcriptome data verified calcitriol-induced upregulation of only a small set of VDRTGs. The molecular network of 1541 calcitriol-responsive VDRTGs showed a significant relationship with leukocyte transendothelial migration, Fcγ receptor-mediated phagocytosis, and transcriptional regulation by VDR, suggesting a pivotal role of genome-wide VDRTGs in immune regulation.

Conclusion: These results suggest the working hypothesis that persistent deficiency of vitamin D might perturb the complex network of VDRTGs in immune cells, being responsible for induction of an autoimmune response causative for MS.

Keywords

ChIP-Seq, GenomeJack, multiple sclerosis, pathway analysis, vitamin D, VDR

Date received: 4th June 2012; revised: 21st November 2012; accepted: 28th November 2012

Introduction

Multiple sclerosis (MS) is an inflammatory demyelinating disease of the central nervous system (CNS) presenting with relapsing–remitting and progressive clinical courses. Pathologically, it is characterized by inflammation, demyelination, gliosis, and axonal degeneration, although underlying molecular mechanisms remain largely unknown. Even genetically identical monozygotic twins express a concordance rate of approximately 30% for MS. This suggests a great contribution of environmental factors to MS pathogenesis, such as cigarette smoking, Epstein Barr virus (EBV) infection, and low serum vitamin D levels.¹

Vitamin D is a liposoluble vitamin essential for calcium metabolism, available from dietary sources and also produced endogenously when the sunlight Ultraviolet B

(UVB) triggers its synthesis in the skin, followed by consecutive hydroxylation in the liver and kidney to generate 1 α ,25-dihydroxyvitamin D₃, a biologically active form named calcitriol. The vitamin D receptor (VDR) is expressed on various cells including immune cells, such as lymphocytes, macrophages, monocytes, and dendritic cells.

Department of Bioinformatics and Molecular Neuropathology, Meiji Pharmaceutical University, Japan.

Corresponding author:

Jun-ichi Satoh, Department of Bioinformatics and Molecular Neuropathology, Meiji Pharmaceutical University, 2-522-1 Noshio, Kiyose, Tokyo 204-8588, Japan.
Email: satoj@my-pharm.ac.jp